NATIONAL ADVISORY COMMITTEE FOR AERONAUTICS

TECHNICAL NOTE 3121

SOME EFFECTS OF ASPECT RATIO AND TAIL LENGTH ON THE CONTRIBUTION OF A VERTICAL TAIL TO UNSTEADY LATERAL DAMPING AND DIRECTIONAL STABILITY OF A MODEL OSCILLATING CONTINUOUSLY IN YAW

By Lewis R. Fisher

Langley Aeronautical Laboratory
Langley Field, Va.

Washington
January 1954

NATIONAL ADVISORY COMMITTEE FOR AERONAUTICS

TECHNICAL NOTE 3121

SOME EFFECTS OF ASPECT RATIO AND TAIL LENGTH ON THE CONTRIBUTION OF A VERTICAL TAIL TO UNSTEADY LATERAL DAMPING AND DIRECTIONAL STABILITY OF A MODEL OSCILLATING CONTINUOUSLY IN YAW

By Lewis R. Fisher

SUMMARY

A fuselage—vertical-tail combination with tails of two aspect ratios, each of which was tested at four tail lengths, was oscillated in yaw through a range of reduced-frequency parameter corresponding to the lateral motions of airplanes. The tail force caused by yawing, and, hence, the approximate contribution of the tail to the damping in yaw, was measured for each condition as a phase angle between the lateral force on the vertical tail and the displacement in yaw of the model. These phase angles were measured with the tail in the presence of the fuselage.

A reduction in the contribution of the vertical tail to the lateral damping took place as the frequency was reduced to low values and became more pronounced as the aspect ratio and tail length were increased.

A complementary theoretical analysis based on the finite-span theory of Biot and Boehnlein indicates certain conditions of tail length, aspect ratio, and reduced-frequency parameter for which the lateral damping of an isolated vertical tail goes to zero and then becomes destabilizing. Although testing within these regions of indicated negative damping was not possible, a condition of negative damping was obtained experimentally in a region of theoretically predicted positive damping.

The analysis indicates that, for each vertical-tail aspect ratio, there is a tail length for which the lateral damping is minimum. This tail position is forward of the center of gravity for small aspect ratios and the higher frequencies and moves rearward with increasing aspect ratios and lower frequencies.

INTRODUCTION

Two of the more important geometric variables which affect the lateral damping of an airplane are the aspect ratio of the vertical tail and the distance between the vertical tail and the airplane center of gravity (or tail length). Although both of these variables have been investigated extensively for steady flight conditions, almost no information is available to indicate any effects of variations in these geometric parameters on the unsteady damping of the vertical tail, that is, the damping during a lateral oscillation. As a result, it is common practice to rely on stability derivatives which generally neglect unsteady-flow effects in the calculation of lateral motions and stability of airplanes and missiles. The existence of an effect of frequency on the damping has been established, both experimentally and theoretically, in a number of investigations (such as ref. 1). An instability such as the small-amplitude undamped lateral oscillation which has been found to occur in the flight behavior of certain present-day airplanes could logically be explained as a change in the lateral damping resulting from frequency effects.

At the time the present investigation was undertaken, a number of published analyses were available on the finite-span theory for oscillating wings. Reference 2 discusses briefly the methods of Reissner and Stevens (ref. 3), Jones (ref. 4), and Biot and Boehnlein (ref. 5). The method of Biot and Boehnlein was selected, at that time, to serve as a basis of comparison with the intended series of experiments because it is rigorous to a degree only slightly less than that of Reissner and Stevens for the case to be studied and was much easier to apply. Moreover, no oversimplifying assumptions regarding the nature of the oscillating wake are made in the method.

Since this investigation was begun, much material has been added to the literature of unsteady air loads. In this material is a simple method for the calculation of the unsteady longitudinal stability derivatives of an airplane developed by Miles (ref. 6). Some of the derivatives evaluated by Miles, in lieu of certain symplifying assumptions, differ from those of the present investigation, which employs the circulation functions of Biot and Boehnlein, in the region where the reduced frequency approaches zero. More recently, a method has been developed by Lawrence and Gerber (ref. 7) which permits the calculation of the unsteady air loads on wings, particularly of the aspect ratios comparable to those employed for conventional vertical tails. Although the method of Biot and Boehnlein was derived as a high-aspect-ratio theory, a comparison with the experimental results of references 2 and 8 indicates that this method yields reasonable results for aspect ratios as low as 2.

In view of the amount of material now available, the method of Biot and Boehnlein appears to be only one of several methods which can be used to calculate the unsteady-circulation functions for the analysis presented

herein. As stated previously, this method was selected because of its availability at the time the analysis was begun and its relative ease of application.

The unsteady-flow theory of Biot and Boehnlein indicates that, at certain low values of the reduced frequency, the damping-in-yaw parameter changes sign and becomes positive. The value of the reduced frequency at which this change occurs varies with tail length and with vertical-tail aspect ratio. The primary purpose of this investigation was to map these regions of predicted negative damping as functions of reduced frequency, tail location, and aspect ratio and to approach these regions experimentally insofar as possible. The regions of indicated instability are generally outside the practical reduced-frequency range for conventional airplanes; however, these regions of indicated instability were based on the aerodynamics of an isolated tail in potential flow. It seemed possible, therefore, that viscous effects or fuselage interference, or both, might alter the vertical-tail damping so that the conditions for zero or negative damping would fall in a practical reduced-frequency region.

The test procedure followed was similar to that in reference 8. The damping in yaw was determined for vertical tails of two aspect ratios and four tail locations, one of which was forward of the assumed center of gravity. The range of reduced-frequency parameter was chosen to include the range commonly encountered in the lateral oscillations of airplanes.

SYMBOLS

The data are referred to the system of stability axes shown in figure 1 and are presented in the form of standard NACA coefficients of forces and moments about a reference point which is located only with respect to the quarter-chord line of the vertical tails (see fig. 2). The coefficients and symbols used herein are defined as follows:

a	nondimensional tail length referred to semichord of vertical tail, $-\left(\frac{l_t}{c_t/2} + 0.5\right)$
A	vertical-tail aspect ratio, b_t^2/S_t
b	span, ft
c	chord, ft
f	frequency, cps

k	reduced-frequency parameter referred to semichord of vertical tail, $\omega c_t/2V$
l_t	distance from moment reference point to assumed center of pressure of vertical tail (positive when tail is rearward of moment reference point), ft
m	mass, slugs
N	yawing moment about origin of axes, ft-lb
P	period of oscillation, sec
q	dynamic pressure, $\rho V^2/2$, lb/sq ft
ρ	mass density of air, slugs/cu ft
S	area, sq ft
t	time, sec
V	free-stream velocity, ft/sec
Y	lateral force, lb
β	angle of sideslip, radians
$\dot{\beta} = \frac{d\beta}{dt}$	
ψ	angle of yaw, radians
r	yawing velocity, $d\psi/dt$, radians/sec
$\dot{r}$	yawing acceleration, $d^2\psi/dt^2$, radians/sec^2
ω	angular velocity, $2\pi f$, radians/sec
ϕ_N	phase angle between yawing moment of vertical tail and displacement in yaw (positive when moment leads displacement)
ϕ_Y	phase angle between lateral force on vertical tail and displacement in yaw (positive when force leads displacement)

$\bar{P}(k) = F + iG$
$\bar{Q}(k) = H + iJ$
} unsteady-circulation functions introduced by Biot and Boehnlein (ref. 5)

C_n yawing-moment coefficient, N/qS_wb_w

C_Y lateral-force coefficient, Y/qS_w

$$C_{n_\beta} = \frac{\partial C_n}{\partial \beta}$$

$$C_{n_{\dot{\beta}}} = \frac{\partial C_n}{\partial \frac{\dot{\beta} b_w}{2V}}$$

$$C_{n_r} = \frac{\partial C_n}{\partial \frac{r b_w}{2V}}$$

$$C_{n_{\dot{r}}} = \frac{\partial C_n}{\partial \frac{\dot{r} b_w^2}{4V^2}}$$

$$C_{Y_\beta} = \frac{\partial C_Y}{\partial \beta}$$

$$C_{Y_{\dot{\beta}}} = \frac{\partial C_Y}{\partial \frac{\dot{\beta} b_w}{2V}}$$

$$C_{Y_r} = \frac{\partial C_Y}{\partial \frac{r b_w}{2V}}$$

$$C_{Y_{\dot{r}}} = \frac{\partial C_Y}{\partial \frac{\dot{r} b_w^2}{4V^2}}$$

Subscripts:

w	wing
t	tail
meas	measured
aerod	aerodynamic

MODEL AND APPARATUS

The fuselage of the model was a hollow circular cylinder 4 inches in diameter and 27 inches long with a wall thickness of 1/8 inch, was constructed of aluminum, and contained an internal mahogany sleeve 9 inches long. This sleeve retained the internal strain-gage side-force balance, described in reference 8, which supported the vertical tail. The cylinder was made in two lengths; either section or both could be employed as needed for varying the tail length. An ogival mahogany fairing of circular cross section enclosed each end of the cylinder.

Two rectangular-plan-form vertical tails with NACA 0012 airfoil sections were constructed of laminated balsa wood. These tails were 12 and 6 inches in span and 4 inches in chord with aspect ratios of 3.0 and 1.5, respectively. Both vertical tails were tested with their quarter-chord lines at distances of 18 and 9 inches rearward of the center of rotation of the model, 9 inches forward of the center of rotation, and directly at the center of rotation. These distances correspond to values of the nondimensional tail-length parameter a of -9.5, -5.0, 4.0, and -0.5, respectively. Figure 2 is a drawing of the model configurations tested; figure 3, a photograph of one of the model configurations on the forced-oscillation strut in the Langley stability tunnel; and figure 4, a photograph of the fuselage-contained strain-gage balance which measured forces on the vertical tail.

Since this model had no wing on which to base the computation of the aerodynamic coefficients, ratios of tail area to wing area S_t/S_w of 0.26 and 0.13 were arbitrarily assumed for the tails of aspect ratios 3.0 and 1.5, respectively. The ratio of the tail chord to wing span c_t/b_w was assumed to be 0.12. For the larger tail, these ratios roughly correspond to those of the models used for the tests of references 2 and 8.

The oscillation and data recording apparatus was the same as the equipment used for the tests of reference 8 and is described in that reference.

TESTS

For each of the four tail lengths and the two vertical-tail aspect ratios, the fuselage—vertical-tail combination was oscillated harmonically in yaw for each of nine frequencies. The nominal values of these frequencies were 0.4, 0.5, 0.7, 1.0, 1.4, 2.0, 2.7, 4.0, and 5.0 cps. These frequencies correspond to a range of the reduced-frequency parameter from 0.003 to 0.036 with the heavier distribution of test points falling in the lower portion of the range covered.

The results of reference 8 indicated that changes in amplitude of oscillation from 4° to $1/2^\circ$ had only a small effect on the lateral damping and that the observations made had the greatest accuracy for the highest amplitudes. In order to obtain the greatest accuracy of test points, the tests in this investigation were made with an amplitude of oscillation of $\pm 4^\circ$. Some of the tests were made with an amplitude of $\pm 2^\circ$ as a check against the possibility of an unexpectedly large effect of amplitude. No such amplitude effect was apparent.

As in previous tests of this nature, the model was tested in an inverted position in order to minimize any strut interference on the vertical tail, and at zero angle of attack with respect to the fuselage center line. All tests were conducted at a dynamic pressure of 24.9 lb/sq ft which under standard sea-level conditions corresponds to a free-stream velocity of 146 fps.

ANALYSIS

Considerations Employed in Reduction of Data

With the model undergoing continuous oscillation in yaw about a pivot located at its assumed center of gravity, the lateral force on the vertical tail and the displacement in yaw of the model were recorded simultaneously as functions of time through a range of reduced-frequency parameter. By the method described in reference 8, the lag between the tail force and the displacement in yaw was measured as a time increment and was converted to a phase angle in degrees by the relationship

$$\phi_{Y_{meas}} = \frac{\Delta t}{P} \times 360 \qquad (1)$$

For a model experiencing such a motion, by assuming small perturbations, the instantaneous lateral force impressed on a strain gage upon which the vertical tail is mounted may be expressed, in the system of stability axes (see fig. 1), as

$$Y = -\left(m l_t + Y_{\dot{\psi}}\right)\ddot{\psi} - \left(Y_{\dot{\psi}} - Y_{\dot{\beta}}\right)\dot{\psi} + Y_{\beta}\psi \tag{2}$$

where the dotted symbols represent the time derivatives of ψ and β. If the motion is harmonic, then

$$\psi = \psi_0 \cos \omega t$$

and if this equation, together with its time derivatives, is substituted into equation (2), the lateral-force coefficient becomes

$$C_Y = \psi_0 \left\{ \left[k^2 \left(\frac{b_w}{c_t}\right)^2 \left(\frac{8 m l_t}{\rho b_w{}^2 S_w} + C_{Y_{\dot{r}}} \right) + C_{Y_\beta} \right] \cos \omega t + \frac{b_w}{c_t} k \left(C_{Y_r} - C_{Y_{\dot{\beta}}} \right) \sin \omega t \right\} \tag{3}$$

The measured phase angle then is expressed as

$$\tan \phi_{Y_{meas}} = \frac{\frac{b_w}{c_t} k \left(C_{Y_r} - C_{Y_{\dot{\beta}}} \right)}{C_{Y_\beta} + k^2 \left(\frac{b_w}{c_t}\right)^2 \left(\frac{8 m l_t}{\rho b_w{}^2 S_w} + C_{Y_{\dot{r}}} \right)} \tag{4}$$

When the mass term in equation (4) is set equal to zero, a purely aerodynamic phase angle is obtained and may be expressed as

$$\tan \phi_{Y_{aerod}} = \frac{\frac{b_w}{c_t} k \left(C_{Y_r} - C_{Y_{\dot{\beta}}} \right)}{C_{Y_\beta} + k^2 \left(\frac{b_w}{c_t}\right)^2 C_{Y_{\dot{r}}}} \tag{5}$$

By simple substitution, equations (4) and (5) can be related to give a mass correction which can be applied to the measured phase angle to obtain the aerodynamic phase angle

$$\tan \phi_{Y_{aerod}} = \left\{ 1 + \frac{8k^2 l_t m}{\rho S_w c_t^2 \left[C_{Y_\beta} + k^2 \left(\frac{b_w}{c_t} \right)^2 C_{Y_{\dot{r}}} \right]} \right\} \tan \phi_{Y_{meas}} \tag{6}$$

The experimental values of the lateral force due to yawing were computed from the aerodynamic phase angles given by equation (5) rearranged in the manner

$$C_{Y_r} - C_{Y_{\dot{\beta}}} = \frac{1}{k} \frac{c_t}{b_w} \left[C_{Y_\beta} + k^2 \left(\frac{b_w}{c_t} \right)^2 C_{Y_{\dot{r}}} \right] \tan \phi_{Y_{aerod}} \tag{7}$$

The oscillatory lateral force due to sideslipping in equations (6) and (7) is a combination of the steady-state lift-curve slope of the vertical tail C_{Y_β} and a force coefficient due to the rotary acceleration of the vertical tail $C_{Y_{\dot{r}}}$. The $C_{Y_{\dot{r}}}$ portion, which is the only component dependent upon frequency, can be shown to be insignificant compared with the C_{Y_β} portion for the tail lengths and the range of frequency now being considered. This term was, therefore, neglected and the steady-state C_{Y_β} alone was used in equations (6) and (7) to obtain the experimental values of $C_{Y_r} - C_{Y_{\dot{\beta}}}$ for this investigation.

Since the damping-in-yaw parameter $C_{n_r} - C_{n_{\dot{\beta}}}$ is of more general interest than the lateral force due to yawing, the experimental results for $C_{Y_r} - C_{Y_{\dot{\beta}}}$ multiplied by a tail-length parameter

$$C_{n_r} - C_{n_{\dot{\beta}}} = -\frac{1}{2} \frac{l_t}{c_t/2} \frac{c_t}{b_w} \left(C_{Y_r} - C_{Y_{\dot{\beta}}} \right) \tag{8}$$

were used to obtain experimental values of the oscillatory damping in yaw. This procedure was followed for each tail length with the exception of the tail length equal to zero where the result obviously would be lacking in significance.

This procedure for determining the experimental unsteady damping in yaw is somewhat different from that used for similar tests of reference 8. For airplanes with conventional tail lengths, such as those of the models in references 2 and 8, the phase angle between the lateral force on the vertical tail and the displacement of the model should be about the same as the phase angle between the yawing moment of the vertical tail and the displacement. In the investigation of reference 8, although the phase angle measured was actually that of the lateral force ϕ_Y, the phase angle was considered to be that of the yawing moment ϕ_N, since the two were about the same for that tail length. For tail lengths near zero, however, such as one of those considered in the present investigation, the phase angle of the lateral force differs greatly from that of the yawing moment. For this reason for the condition of zero tail length, the phase angle was not interpreted in terms of yawing moment. This phenomenon is discussed further in the next section.

Theoretical Calculations

The phase angle of the lateral force can be calculated from unsteady-lift theory in the manner in which the yawing-moment phase angle was obtained theoretically in reference 8. The lateral-force derivatives for the two-dimensional vertical tail are presented in the appendix of reference 2. These equations also represent the finite-span derivatives when the F and G unsteady-circulation functions used are the finite-span functions of reference 5. These derivatives are

$$\left.\begin{aligned} C_{Y_\beta} &= -2\pi \frac{S_t}{S_w} F \\ C_{Y_{\dot\beta}} &= -\pi \frac{S_t}{S_w} \frac{c_t}{b_w}\left(1 + 2\frac{G}{k}\right) \\ C_{Y_r} &= 2\pi \frac{S_t}{S_w} \frac{c_t}{b_w} F\left(\frac{1}{2} - a\right) \\ C_{Y_{\dot r}} &= -\pi \frac{S_t}{S_w}\left(\frac{c_t}{b_w}\right)^2 \left[a - \frac{2G}{k}\left(\frac{1}{2} - a\right)\right] \end{aligned}\right\} \qquad (9)$$

The oscillatory lateral force due to yawing for the motion herein considered where $\beta = -\psi$ is

$$C_{Y_r} - C_{Y_{\dot{\beta}}} = 2\pi \frac{S_t}{S_w} \frac{c_t}{b_w} \left[\left(\frac{1}{2} - a \right) F + \frac{G}{k} + \frac{1}{2} \right] \tag{10}$$

and the oscillatory lateral force due to sideslipping is

$$C_{Y_\beta} + k^2 \left(\frac{b_w}{c_t} \right)^2 C_{Y_{\dot{r}}} = -\pi \frac{S_t}{S_w} \left[ak^2 + 2F + (2a - 1)kG \right] \tag{11}$$

If equations (10) and (11) are combined with equation (5), the theoretical phase angle is seen to be

$$\tan \phi_{Y_{aerod}} = \frac{B_1}{A_1} \tag{12}$$

where

$$A_1 = ak^2 + 2F + (2a - 1)kG$$

and

$$B_1 = (2a - 1)kF - 2G - k$$

The phase angle of the yawing moment, which was employed in reference 8, is given by

$$\tan \phi_{N_{aerod}} = \frac{B_0}{A_0}$$

where

$$A_0 = (2a - 1)akG + \left(a - \frac{1}{2}\right)kJ + \left(a^2 + \frac{1}{8}\right)k^2 + 2aF + H$$

$$B_0 = (2a - 1)akF + \left(a - \frac{1}{2}\right)kH - \left(a - \frac{1}{2}\right)k - 2aG - J$$

and F, G, H, and J are the unsteady-circulation functions of reference 5. In reference 2 the unsteady directional stability is shown to be proportional to A_0 and the unsteady damping in yaw is shown to be proportional to B_0/k in the following manner:

$$C_{n_\beta} + k^2\left(\frac{b_w}{c_t}\right)^2 C_{n_{\dot{r}}} = -\frac{\pi}{2}\frac{c_t}{b_w}\frac{S_t}{S_w}A_0$$

$$C_{n_r} - C_{n_{\dot{\beta}}} = -\frac{\pi}{2}\left(\frac{c_t}{b_w}\right)^2\frac{S_t}{S_w}\frac{B_0}{k}$$

The important difference encountered between ϕ_Y and ϕ_N lies in the result that, for a value of the tail-length parameter near zero, A_0 goes to zero but B_0 remains finite. For all finite values of k, then, tan ϕ_N becomes infinite for $a \approx 0$. This result does not occur in the consideration of ϕ_Y since A_1 is finite for all values of a. Physically, this result means simply that the directional stability goes to zero for a tail length close to zero, whereas the lateral force due to sideslipping does not. The theoretical effects of tail length upon the damping in yaw and the directional stability are discussed more completely in the next section.

RESULTS AND DISCUSSION

The experimental results of this investigation are shown as the effects of reduced-frequency parameter, tail length, and tail aspect ratio on the phase angle in figure 5, on the lateral force due to yawing in figure 6, and on the damping in yaw in figure 7. For the most part, this discussion is confined to the effects of the test variables on the

yawing derivatives rather than the lateral-force derivatives, since the damping in yaw and the directional stability are the chief parameters which dictate the yawing motions of an airplane.

In figure 5, the phase angle is seen to vary almost linearly for all tail lengths and both aspect ratios, although the slopes of these variations are more negative than those indicated by equation (12) in which the unsteady-circulation functions of reference 5 are used.

The lateral forces due to yawing in figure 6 exhibit the trends predicted by the theory of reference 5 in that $C_{Y_r} - C_{Y_{\dot{\beta}}}$ undergoes a small negative change as the reduced-frequency parameter decreases. At a small value of k, the negative change in $C_{Y_r} - C_{Y_{\dot{\beta}}}$ becomes very abrupt. The reduced-frequency parameter at which this abrupt change occurs is much higher than the theory predicts - it is, in fact, in the practical frequency range for airplanes. At zero reduced frequency, the theoretical values of $C_{Y_r} - C_{Y_{\dot{\beta}}}$ go to negative infinity for all aspect ratios and tail lengths. The frequency effects on $C_{Y_r} - C_{Y_{\dot{\beta}}}$ are seen to become more marked as the aspect ratio is increased. A variation in tail length has no noticeable effect on the variation of $C_{Y_r} - C_{Y_{\dot{\beta}}}$ with reduced-frequency parameter. The F term in equation (10), which is the C_{Y_r} portion, is the important term in the equation and does not vary appreciably with frequency for this small frequency range. At low frequencies, however, the $C_{Y_{\dot{\beta}}}$ component, which depends on G/k, becomes increasingly important and, in fact, introduces a singularity in the expression when $k = 0$.

The damping in yaw in figure 7 reflects, of course, the lateral force due to yawing since the two are related by the tail length. The abrupt reduction in the lateral damping is again apparent in figure 7 as the reduced-frequency parameter approaches zero. This effect is especially marked for the higher aspect-ratio tail. In fact, the damping for the $A = 3$ tail at a tail length of $a = -5$ decreased through zero and became negative damping for two test points at the lowest frequencies. In general, the predicted effects of aspect ratio and tail length on the variation of the lateral damping with reduced-frequency parameter are well-substantiated by the experimental data.

Although the theoretical damping approaches positive infinity at $k = 0$ for positive tail lengths (negative values of a), the theory indicates that the damping approaches negative infinity at $k = 0$ for negative tail lengths. In other words, the theory, based on the unsteady-circulation functions of reference 5, indicates that, with the vertical tail forward of the center of gravity, the lateral damping should increase

steadily as the reduced frequency goes to small values, rather than a reduction in damping which occurs with the vertical tail in the normal location. The experiments with the $A = 3$ tail at $a = 4$ showed an abrupt increase in stability for one portion of the frequency range as the reduced frequency became smaller.

Some sizable differences in magnitude of $\phi_{Y_{aerod}}$, $C_{Y_r} - C_{Y_{\dot{\beta}}}$, and $C_{n_r} - C_{n_{\dot{\beta}}}$ exist between the experimental and the calculated results for some of the test conditions. These differences may be at least partially explained by the end-plate effect of the fuselage on the vertical tail which would normally make the effective aspect ratio of the tail larger than the geometric aspect ratio. The geometric aspect ratios were used for all calculated results. For the low-aspect-ratio region being considered, small changes in aspect ratio can create sizable differences in magnitude of both the inphase and the out-of-phase forces on the vertical tail.

Some error may have been introduced in the experimental results by a distortion of the vertical tail under large loads. This distortion was most apparent for the high-aspect-ratio tail at the longest tail length.

The combinations of tail length, aspect ratio, and reduced-frequency parameter for which the calculated lateral damping of the vertical tail becomes zero are shown in figure 8. The ticked side of each curve is in the region where the quantity $C_{n_r} - C_{n_{\dot{\beta}}}$ is positive and signifies an unstable condition. The reduced frequencies for which the instability occurs for the usual vertical-tail aspect ratios appear to be considerably lower than those which correspond to the lateral motions of airplanes. Although testing within these regions of predicted instability was not possible because of the very low frequencies required for a reasonable aspect ratio, the fact that one case of negative damping was obtained experimentally signifies that consideration of a nonpotential type of flow may extend these regions of instability to higher frequencies than indicated by the potential theory. For one tail length, $a = -1.25$, the greatest range of frequency exists for each aspect ratio for which the lateral damping can become negative.

In figure 9 is shown the variation of ϕ_Y/k $\left(\text{approximately equal to } B_1/kA_1\right)$ with tail-length parameter for a representative value of the reduced-frequency parameter, $k = 0.05$. Since A_1 and B_1/k are linear functions of tail length, ϕ_Y/k is, of course, almost linear as well. The function ϕ_N/k would have the same variation with a with the exception of a small interval near $a = -0.5$ where a singularity would occur and the function becomes infinite.

The variation of the damping in yaw with tail-length parameter is shown in figure 10 for the representative reduced-frequency parameter $k = 0.05$ which is beyond the regions of indicated instability in figure 8. The damping in yaw is represented in figure 10 as

$$\frac{B_O}{k} = -\frac{2}{\pi}\left(\frac{b_w}{c_t}\right)^2 \frac{S_w}{S_t}\left(C_{n_r} - C_{n_{\dot{\beta}}}\right)$$

In terms of the unsteady-circulation functions, the damping parameter is also

$$\frac{B_O}{k} = (2a - 1)aF + \left(a - \frac{1}{2}\right)H - \left(a - \frac{1}{2}\right) - \frac{2aG}{k} - \frac{J}{k}$$

These equations are developed in reference 2 on the basis of the method of reference 5; this method is summarized briefly in the appendix to this paper. The tables of the unsteady-circulation functions presented in reference 5 are also extended to the low values of reduced-frequency parameter commonly encountered in the lateral oscillations of airplanes. All experimental values for $k = 0.05$ are extrapolated from the test results.

A point of interest revealed in figure 10 is that, as the aspect ratio becomes smaller, the lateral damping reaches a minimum for each aspect ratio at values of the tail-length parameter which become progressively more positive. This effect is shown to greater advantage in figure 11 in which the tail-length parameter for minimum damping for each aspect ratio is given. This tail length for minimum damping is given as a function of aspect ratio and reduced-frequency parameter by

$$a = \frac{F - H + \frac{2G}{k} + 1}{4F}$$

Similar curves are obtained for each of three values of the reduced frequency which encompass the stability range of reduced frequencies. For vertical tails of commonly employed aspect ratios, minimum damping is obtained for locations forward of the airplane center of gravity. As the aspect ratio is increased and the frequency of oscillation becomes low, the tail location for minimum damping shifts rearward.

The directional-stability parameter

$$A_0 = -\frac{2}{\pi}\frac{b_w}{c_t}\frac{S_w}{S_t}\left[C_{n_\beta} + C_{n_{\dot{r}}}k^2\left(\frac{b_w}{c_t}\right)^2\right]$$

is represented as a function of tail-length parameter in figure 12. The experimental values in this figure are obtained from static sideslip tests. It was shown in reference 2 that, for the tail lengths given, frequency has no appreciable effect on the directional stability in this low range of reduced frequency and for these small aspect ratios. In terms of the unsteady-circulation functions, the directional stability (ref. 2) is

$$A_0 = (2a - 1)akG + \left(a - \frac{1}{2}\right)kJ + \left(a^2 + \frac{1}{8}\right)k^2 + 2aF + H$$

which is a quadratic function of the tail length. When both roots of this quadratic equation are determined, one root is the small value of a which corresponds to those shown in figure 12, whereas the other is a very large value of a.

The variation of the directional-stability parameter with extremely large values of the tail-length parameter is presented in figure 13. Any discussion of such extreme tail lengths is, of course, of only academic interest, but the trends indicated are at least worthy of note. Normally, the directional stability due to the vertical tail would be expected to be zero only when the tail length is about zero. However, in the oscillatory case, the directional-stability parameter is a combination of a component proportional to displacement C_{n_β} and one proportional to the rotary acceleration $C_{n_{\dot{r}}}$; these components are 180° out of phase. The C_{n_β} portion is a linear function of tail length and is the stability parameter considered in the static case. The $C_{n_{\dot{r}}}$ portion of the directional-stability parameter is a function of the square of the tail length. When the tail length becomes of sufficient magnitude, as shown in figure 13, the steady portion of the stability parameter becomes insignificant compared with the unsteady portion. Only for an aspect ratio of $5\frac{1}{3}$, for $k = 0.05$, is the stability parameter linear with tail length for all tail lengths; for all other aspect ratios, the curves are parabolic in the fashion shown and the stability parameter changes sign for an extremely large tail length as well as for one near zero.

Some similar remarks may be made with regard to the unsteady lift-curve slope of the vertical tail $C_{Y_\beta} - C_{Y_{\dot{r}}}$. Tail location alone would not be expected to produce any effect on the steady-state portion C_{Y_β}. For a sufficiently long tail length, however, the unsteady lift produced by the plunging acceleration of the vertical tail could cause the total lateral force due to sideslipping to go to zero. At this tail length, of course, the stability parameter will also be zero.

CONCLUDING REMARKS

An experimental investigation of the effects of tail length and aspect ratio on the unsteady lateral damping of a vertical tail in the presence of a fuselage indicated that a reduction in damping took place as the frequency was reduced to low values and became more pronounced for the longer tail lengths and the larger aspect ratio tested. For one tail-length and aspect-ratio combination, a condition of negative damping was encountered at the lowest frequencies tested. This test condition was in a region where the unsteady potential-flow theory predicts positive damping for an isolated vertical tail.

A complementary theoretical analysis of these geometrical effects, based on the finite-span unsteady-lift theory of Biot and Boehnlein, indicates that, for each aspect ratio, there is a tail length for which the lateral damping will be minimum. The tail position for minimum damping is forward of the moment reference point for small aspect ratios and higher frequencies but moves to a location rearward of the reference point with increasing aspect ratio and lower frequencies. For an airplane configuration being oscillated forceably in yaw at a reduced frequency comparable to those investigated, the aerodynamic-directional-stability term can be decreased in magnitude as a result of an increase in the component due to the lateral acceleration of the vertical tail as the tail length goes to large values. For sufficiently long tail lengths, this term can go to zero and then change sign.

Langley Aeronautical Laboratory,
National Advisory Committee for Aeronautics,
Langley Field, Va., September 23, 1953.

APPENDIX

COMPUTATIONAL METHOD OF BIOT AND BOEHNLEIN

A concise summary is presented of the procedure developed in reference 5 for computing the finite-span circulation functions for use where a good approximation of the unsteady forces and moments on an oscillating surface is sufficient, for example, in stability calculations. The tables of the circulation functions and intermediate functions presented in reference 5 are also extended to the low values of the reduced-frequency parameter usually considered in stability investigations.

The forces and moments on the complete oscillatory wing are obtained by a spanwise integration of the expressions that result from satisfying the boundary conditions at the midspan position on the wing. Comparative calculations made for the investigation of reference 2 indicate that, for the range of reduced-frequency parameter being considered and for aspect ratios of the order of 2 and greater, this one-point approximation yields about the same results as the more extensive procedure whereby the computation is made for several points along the span (ref. 3, for example). The assumption of an elliptic loading, then, does little to compromise the accuracy of the computation for stability purposes but does greatly simplify the procedure.

In reference 5, the equations for the lift L and the pitching moment $M_{c/2}$ per unit span for an airfoil oscillating in pitch about its midchord point are shown to be

$$L = \pi\rho cV\dot{h}\left(\frac{ik}{2} + \bar{P}\right) + \pi\rho cV^2\alpha\left[\frac{ik}{2} + \left(1 + \frac{ik}{2}\right)\bar{P}\right] \tag{A1}$$

and

$$M_{c/2} = \frac{\pi}{4}\rho c^2V\dot{h}\bar{Q} + \frac{\pi}{4}\rho c^2V^2\alpha\left[\frac{k^2}{8} - \frac{ik}{2} + \left(1 + \frac{ik}{2}\right)\bar{Q}\right] \tag{A2}$$

where $\dot{h}$ is the instantaneous vertical velocity of the midchord point (positive downward), α is the instantaneous angle of attack (positive when nose up), and upward lift and nose-up pitching moment are positive.

By using these equations, the total yawing moment of a vertical tail about the center of gravity of an airplane N_{cg} is given by

$$N_{cg} = M_{c/2} - L\left(l_t + \frac{c_t}{4}\right) \tag{A3}$$

where $M_{c/2}$ is the pitching moment about the midchord of the vertical tail as expressed by equation (A2), L is the lift on the vertical tail given by equation (A1), and l_t is the tail length. Substituting equations (A1) and (A2) into equation (A3), nondimensionalizing the resulting expression, and setting it equal to an equation for the same quantity which is written in terms of the stability derivatives C_{n_β}, $C_{n_{\dot\beta}}$, C_{n_r}, and $C_{n_{\dot r}}$ results in expressions for the lateral damping and the directional stability of the vertical tail derived as functions of the finite-span circulation functions $\bar{P}$ and $\bar{Q}$. This procedure was used in the investigation of reference 2.

In the resulting equations, $\bar{P}$ and $\bar{Q}$ are complex functions whose real and imaginary parts may be computed for any aspect ratio and value of reduced frequency k as outlined below.

The following functions, which are dependent only upon aspect ratio, are required first (the notation for the most part is that of ref. 5):

$$a_0 = \frac{4}{3A}\sqrt{A^2 + 9} - \frac{4}{3}$$

$$a_1 = \frac{20}{A}\sqrt{A^2 + 1} + \frac{32}{A\sqrt{A^2 + 4}} - \frac{4}{A}\sqrt{A^2 + 9} - \frac{16}{A\sqrt{A^2 + 16}} - 16$$

and

$$a_2 = -\frac{24}{A}\sqrt{A^2 + 1} - \frac{32}{A\sqrt{A^2 + 4}} + \frac{8}{3A}\sqrt{A^2 + 9} + \frac{32}{A\sqrt{A^2 + 16}} + \frac{64}{3}$$

Table I, which was taken from reference 5 with some minor corrections, gives the values of a_0, a_1, and a_2 for a range of aspect ratio. The variation of these functions with aspect ratio is shown in figure 14.

Two functions required, which depend only on frequency, are

$$Q_0 = -\frac{\pi k}{2}\left\{J_0(k)\cos k + Y_0(k)\sin k + i\left[J_0(k)\sin k - Y_0(k)\cos k\right]\right\}$$

and

$$Q_1 = -\frac{\pi k}{2}\left\{J_1(k)\sin k - Y_1(k)\cos k - i\left[J_1(k)\cos k + Y_1(k)\sin k\right]\right\}$$

where $J_n(k)$ and $Y_n(k)$ are the Bessel functions of the first and the second kinds, respectively, of order n and of argument k. A presentation of the values of Q_0 and Q_1 for low values of the reduced-frequency parameter is given in table II and I and R denote imaginary and real parts, respectively, of Q_0 and Q_1. Figure 15 shows these variations graphically.

The next computation necessary is

$$F = F_c + F_t + F_s$$

where

$$F_c = \frac{1}{16}\left(8a_0 + 2a_1 + a_2\right)$$

$$F_t = \frac{e^{-4/A}}{A\left(1 + \frac{iAk}{4}\right)}\left\{\frac{1}{1 + \frac{iAk}{4}}\left[I_0\left(\frac{4}{A}\right) + I_1\left(\frac{4}{A}\right)\right] + I_0\left(\frac{4}{A}\right) + 2I_1\left(\frac{4}{A}\right)\right\}$$

and

$$F_s = -\frac{2.2716ik}{1 + 3iAk} e^{-1/3A}\left[I_0\left(\frac{1}{3A}\right) + I_1\left(\frac{1}{3A}\right)\right]$$

The functions I_n are the modified Bessel functions of the first kind of order n and of the argument indicated. Two similar functions needed also are

$$F_0 = F_{0c} + F_{0t} + F_{0s}$$

and

$$F_1 = F_{1c} + F_{1t} + F_{1s}$$

where

$$F_{0c} = -\frac{1}{128}(a_1 + a_2)$$

$$F_{1c} = \frac{1}{128}(16a_0 + 8a_1 + 5a_2)$$

$$F_{0t} = \frac{e^{-4/A}}{16\left(1 + \frac{iAk}{4}\right)}\left\{\frac{1}{1 + \frac{iAk}{4}}\left[I_0\left(\frac{4}{A}\right) - \frac{A}{2} I_1\left(\frac{4}{A}\right)\right] + \frac{4}{A}\left[(1 + A)I_0\left(\frac{4}{A}\right) - \left(1 + \frac{A}{2} + \frac{A^2}{2}\right)I_1\left(\frac{4}{A}\right)\right]\right\}$$

$$F_{1t} = \frac{e^{-4/A}}{1 + \frac{iAk}{4}}\left[\frac{\frac{1}{8} I_1\left(\frac{4}{A}\right)}{1 + \frac{iAk}{4}} - \frac{1}{2A} I_0\left(\frac{4}{A}\right) + \left(\frac{1}{2A} + \frac{3}{8}\right)I_1\left(\frac{4}{A}\right)\right]$$

$$F_{0s} = -\frac{1.7037iAk}{1 + 3iAk} e^{-1/3A}\left[I_0\left(\frac{1}{3A}\right) - 6AI_1\left(\frac{1}{3A}\right)\right]$$

and

$$F_{1s} = -\frac{3.4074iAk}{1 + 3iAk} e^{-1/3A} I_1\left(\frac{1}{3A}\right)$$

The circulation functions can now be computed by the following expressions:

$$\bar{P} = F + iG$$

$$\bar{P} = \frac{Q_1 + 2ikF_1}{Q_0 + Q_1 - F}$$

and

$$\bar{Q} = H + iJ$$

$$\bar{Q} = \frac{Q_1 - F + 4F_1 - 4ikF_0}{Q_0 + Q_1 - F}$$

Extensions of the tables of finite-span circulation functions presented in reference 5 to low values of the reduced-frequency parameter are given in tables III to VI and shown in figures 16 to 19.

In two dimensions, equations (A1) and (A2) for the lift and moment reduce to the well-known expressions given by Theodorsen (ref. 9) when the center of rotation of the airfoil section is at the origin of axes (the semichord point). For the two-dimensional case, the expressions for F, F_0, and F_1 become zero, whereupon

$$\bar{P} = \bar{Q} = \frac{Q_1}{Q_0 + Q_1}$$

and

$$\bar{P} = \frac{J_1(J_1 + Y_0) + Y_1(Y_1 - J_0)}{(J_1 + Y_0)^2 + (Y_1 - J_0)^2} - \frac{i(J_0J_1 + Y_0Y_1)}{(J_1 + Y_0)^2 + (Y_1 - J_0)^2}$$

with the Bessel functions of the argument k. This equation is, of course, also the equation given in reference 9 by Theodorsen for the function $C(k) = F + iG$.

For small values of k (substantially, $0 < k < 0.001$) in two dimensions,

$$F = H \approx 1$$

and

$$G = J \approx \frac{\pi}{2} kY_0(k)$$

The latter approximation approaches zero in the manner of $k \log k$. The ratios G/k and J/k, upon which the damping depends, therefore, approach $-\infty$ in the manner of $\log k$ as k goes to zero as is pointed out in reference 10.

For the finite aspect ratios, the imaginary parts of $\bar{P}$ and $\bar{Q}$ still go to zero as k becomes zero. The ratios G/k and J/k become $-\infty$ as k becomes zero as they do in two dimensions, that is, in the manner of $\log k$. The damping, therefore, which is a negative function of G/k and J/k, approaches positive infinity as k goes to zero for a normal positive tail length as it does in the two-dimensional case. A difference exists, however, in the rate of approach of the damping function to infinity. As the aspect ratio is decreased, the divergence of the function takes place at values of k which become closer to zero. For finite aspect ratios, reasonable values of the damping can be calculated for small values of k, except for those very close to zero.

REFERENCES

1. Cicala, P.: Comparison of Theory With Experiment in the Phenomenon of Wing Flutter. NACA TM 887, 1939.

2. Bird, John D., Fisher, Lewis R., and Hubbard, Sadie M.: Some Effects of Frequency on the Contribution of a Vertical Tail to the Free Aerodynamic Damping of a Model Oscillating in Yaw. NACA TN 2657, 1952.

3. Reissner, Eric, and Stevens, John E.: Effect of Finite Span on the Airload Distributions for Oscillating Wings. II - Methods of Calculation and Examples of Application. NACA TN 1195, 1947.

4. Jones, Robert T.: The Unsteady Lift of a Wing of Finite Aspect Ratio. NACA Rep. 681, 1940.

5. Biot, M. A., and Boehnlein, C. T.: Aerodynamic Theory of the Oscillating Wing of Finite Span. GALCIT Rep. No. 5, Sept. 1942.

6. Miles, John W.: The Application of Unsteady Flow Theory to the Calculation of Dynamic Stability Derivatives. Aerophysics Lab. Rep. AL-957, North American Aviation Inc., Sept. 8, 1950.

7. Lawrence, H. R., and Gerber, E. H.: The Aerodynamic Forces on Low Aspect Ratio Wings Oscillating in an Incompressible Flow. Jour. Aero. Sci., vol. 19, no. 11, Nov. 1952, pp. 769-781. (Errata issued, vol. 20, no. 4, Apr. 1953, p. 296.)

8. Fisher, Lewis R., and Wolhart, Walter D.: Some Effects of Amplitude and Frequency on the Aerodynamic Damping of a Model Oscillating Continuously in Yaw. NACA TN 2766, 1952.

9. Theodorsen, Theodore: General Theory of Aerodynamic Instability and the Mechanism of Flutter. NACA Rep. 496, 1935.

10. Heilenday, Frank, Jr., and Rauscher, Manfred: Theoretical and Experimental Methods of Flutter Analysis. Phase 7 - Details of Density Variation Method of Flutter Analysis. Vol. VI (Contract No. NOa(s)8790, Bur. Aero.), M.I.T., June 15, 1949.

TABLE I.- VALUES OF a_0, a_1, AND a_2 FOR A RANGE OF ASPECT RATIO

[From ref. 5]

A	a_0	a_1	a_2
1	2.883037	10.065426	-10.724747
1.5	1.6480907	5.129194	-5.087805
2	1.0703676	3.017580	-2.771230
3	.5522847	1.3167312	-1.0187194
4	.3333334	.6972756	-.4466077
5	.2215873	.4200106	-.2210573
6	.15737865	.2772132	-.1199667
7	.1172900	.19560650	-.06999884
8	.09066729	.1451070	-.0432964
9	.07212334	.11185594	-.0280890
10	.05870753	.0888582	-.0189596
11	.04869749	.0723089	-.0132311
12	.04103521	.0600082	-.0094990

TABLE II.- VALUES OF Q_0 AND Q_1 AS FUNCTIONS OF REDUCED-FREQUENCY PARAMETER

$$\left[Q_0 = R(Q_0) + iI(Q_0);\ Q_1 = R(Q_1) + iI(Q_1)\right]$$

k	$R(Q_0)$	$I(Q_0)$	$R(Q_1)$	$I(Q_1)$
0	0	0	-1.000000	0
.00001	-.000016	-.000115	-1.000000	-.000010
.0001	-.000157	-.000933	-1.000000	-.000100
.0010	-.001564	-.007025	-1.000004	-.000999
.0015	-.002341	-.009931	-1.000007	-.001498
.002	-.003116	-.012667	-1.000012	-.001997
.003	-.004659	-.017789	-1.000025	-.002993
.004	-.006193	-.022574	-1.000041	-.003988
.005	-.007718	-.027110	-1.000062	-.004981
.006	-.009236	-.031447	-1.000085	-.005972
.007	-.010746	-.035620	-1.000113	-.006962
.008	-.012249	-.039652	-1.000143	-.007951
.009	-.013745	-.043563	-1.000176	-.008938
.010	-.015235	-.047364	-1.000212	-.009924
.012	-.018194	-.054685	-1.000292	-.011891
.014	-.021129	-.061683	-1.000383	-.013853
.016	-.024040	-.068406	-1.000483	-.015808
.018	-.026928	-.074889	-1.000593	-.017758
.020	-.029796	-.081161	-1.000712	-.019703
.030	-.043833	-.110008	-1.001425	-.029345
.040	-.057425	-.135728	-1.002315	-.038856
.050	-.070623	-.159183	-1.003355	-.048244
.060	-.083467	-.180879	-1.004528	-.057513
.070	-.095987	-.201146	-1.005819	-.066667
.080	-.108210	-.220219	-1.007215	-.075711
.090	-.120156	-.238271	-1.008706	-.084649
.100	-.131845	-.255436	-1.010284	-.093482

TABLE III.- CIRCULATION FUNCTION F

[Real part of $\bar{F} = F + iG$]

k	Values of F										
	A = 1	A = 1½	A = 2	A = 3	A = 4	A = 5	A = 6	A = 8	A = 10	A = 12	A = ∞
0.00001	0.2512769	0.3447462	0.4218327	0.5382668	0.6192945	0.6775743	0.7210011	0.7808232	0.8198061	0.8471168	0.9999843
.0001	.2512680	.3447294	.4218076	.5382258	.6192403	.6775095	.7209275	.7807369	.8197108	.8470160	.9998421
.0010	.2511793	.3445626	.4215579	.5378208	.6187066	.6768729	.7202100	.7799031	.8188015	.8460539	.9983826
.0015	.2511307	.3444714	.4214219	.5376002	.6184168	.6765297	.7198257	.7794631	.8183274	.8455595	.9975516
.0020	.2510821	.3443804	.4212863	.5373829	.6181332	.6761952	.7194529	.7790395	.8178765	.8450945	.9967096
.0025	.2510339	.3442903	.4211525	.5371690	.6178550	.6758696	.7190910	.7786338	.8174482	.8446597	.9958582
.003	.2509862	.3442011	.4210202	.5369585	.6175828	.6755513	.7187398	.7782448	.8170437	.8442541	.9949986
.004	.2508917	.3440251	.4207603	.5365464	.6170549	.6749404	.7180718	.7775172	.8163025	.8435256	.9932579
.005	.2507982	.3438523	.4205057	.5361485	.6165494	.6743623	.7174482	.7768549	.8156480	.8429042	.9914931
.006	.2507062	.3436824	.4202573	.5357634	.6160675	.6738162	.7168669	.7762565	.8150770	.8423810	.9897082
.008	.2505257	.3433523	.4197780	.5350332	.6151683	.6728222	.7158306	.7752427	.8141614	.8416013	.9860897
.010	.2503498	.3430340	.4193211	.5343344	.6143560	.6719505	.7149528	.7744489	.8135124	.8411034	.9824215
.012	.2501783	.3427272	.4188864	.5337266	.6136277	.6711958	.7142228	.7738494	.8130765	.8408115	.9787174
.016	.2498488	.3421484	.4180821	.5326157	.6124060	.6700062	.7131507	.7731109	.8126328	.8405386	.9712418
.020	.2495359	.3416136	.4173606	.5316871	.6114693	.6691858	.7125028	.7727817	.8124500	.8402857	.9637252
.024	.2492390	.3411207	.4167188	.5309268	.6107826	.6686657	.7121603	.7726473	.8122325	.8397444	.9562111
.028	.2489570	.3406679	.4161506	.5303185	.6103062	.6683728	.7120120	.7725269	.8117906	.8387710	.9487308
.032	.2486899	.3402538	.4156530	.5298469	.6100035	.6682401	.7119629	.7722961	.8110290	.8373453	.9413079
.036	.2484365	.3398757	.4152216	.5294955	.6098371	.6682049	.7119305	.7718732	.8099158	.8354984	.9339603
.040	.2481962	.3395329	.4148517	.5292487	.6097713	.6682154	.7118520	.7712164	.8084645	.8332965	.9267018
.050	.2476507	.3388163	.4141676	.5289879	.6098492	.6681655	.7111859	.7685055	.8035980	.8266840	.9090090
.060	.2471766	.3382800	.4137746	.5290599	.6099666	.6676750	.7096299	.7644759	.7975215	.8191787	.8920397
.080	.2464174	.3376514	.4136131	.5294961	.6094009	.6648013	.7040067	.7540289	.7838582	.8035211	.8604318
.100	.2458691	.3374625	.4139225	.5295744	.6072776	.6597364	.6962206	.7423946	.7700401	.7884014	.8319241
.200	.2449220	.3385051	.4143510	.5198814	.5843244	.6260538	.6548728	.6914701	.7128477	.7258453	.7275799
.400	.2434687	.3346994	.4027834	.4920001	.5456307	.5798906	.6023137	.6263932	.6359688	.6391698	.6249763
.600	.2384715	.3263252	.3904863	.4745514	.5240731	.5534062	.5704542	.5854064	.5896619	.5904088	.5788016
.800	.2312926	.3178151	.3809902	.4636185	.5101118	.5354472	.5489943	.5599369	.5629139	.5634799	.5541466
1.000	.2230196	.3097608	.3734335	.4559483	.5000502	.5227469	.5345063	.5440067	.5468084	.5475235	.5394348

TABLE IV.- CIRCULATION FUNCTION -G

[Negative imaginary part of $\bar{F} = F + iG$]

k	Values of -G										
	A = 1	A = $1\frac{1}{2}$	A = 2	A = 3	A = 4	A = 5	A = 6	A = 8	A = 10	A = 12	A = ∞
0.00001	0.0000072	0.0000114	0.0000160	0.0000252	0.0000330	0.0000394	0.0000445	0.0000520	0.0000573	0.0000611	0.0001151
.0001	.0000561	.0000875	.0001215	.0001887	.0002463	.0002932	.0003310	.0003871	.0004260	.0004544	.0009523
.0010	.0004357	.0006013	.0008044	.0012181	.0015782	.0018723	.0021100	.0024630	.0027087	.0028882	.0070017
.0015	.0006152	.0008296	.0010981	.0016503	.0021330	.0025279	.0028474	.0033225	.0036538	.0038965	.0098776
.0020	.0007839	.0010376	.0013615	.0020330	.0026223	.0031053	.0034964	.0040790	.0044865	.0047863	.0125797
.0025	.0009447	.0012306	.0016024	.0023789	.0030631	.0036248	.0040801	.0047600	.0052374	.0055906	.0151455
.003	.0010992	.0014117	.0018253	.0026957	.0034653	.0040984	.0046123	.0053818	.0059249	.0063297	.0176028
.004	.0013931	.0017456	.0022287	.0032604	.0041791	.0049380	.0055566	.0064895	.0071569	.0076639	.0222566
.005	.0016712	.0020496	.0025875	.0037527	.0047983	.0056663	.0063774	.0074604	.0082495	.0088633	.0266298
.006	.0019369	.0023300	.0029110	.0041881	.0053436	.0063086	.0071042	.0083310	.0092449	.0099753	.0307752
.008	.0024386	.0028353	.0034751	.0049265	.0062647	.0073992	.0083508	.0098652	.0110541	.0120608	.0385130
.010	.0029095	.0032826	.0039551	.0055295	.0070162	.0083018	.0094044	.0112287	.0127446	.0140964	.0456321
.012	.0033561	.0036844	.0043642	.0060298	.0076437	.0090737	.0103335	.0125079	.0144141	.0161820	.0523015
.016	.0041927	.0043832	.0050338	.0068057	.0086443	.0103755	.0119956	.0150298	.0179093	.0206842	.0644043
.020	.0049710	.0049755	.0055520	.0073754	.0094366	.0115197	.0135890	.0177092	.0217687	.0256745	.0752079
.024	.0057045	.0054876	.0059601	.0078073	.0101269	.0126376	.0152553	.0206566	.0260035	.0310298	.0849491
.028	.0064021	.0059574	.0062866	.0081594	.0107867	.0138102	.0170698	.0238845	.0305230	.0365627	.0937910
.032	.0070703	.0063379	.0065521	.0084666	.0114651	.0150855	.0190632	.0273509	.0352043	.0421024	.1018541
.036	.0077139	.0066989	.0067728	.0087572	.0121950	.0164877	.0212364	.0309891	.0399298	.0475204	.1092323
.040	.0083367	.0070282	.0069612	.0090523	.0129974	.0180240	.0235714	.0347263	.0446035	.0527335	.1160013
.050	.0098217	.0077520	.0073535	.0099035	.0153803	.0223998	.0299160	.0440868	.0556549	.0646189	.1306444
.060	.0112298	.0083882	.0077188	.0110168	.0182916	.0273239	.0365688	.0529242	.0654470	.0747983	.1425944
.080	.0139036	.0095790	.0086255	.0141417	.0251870	.0376076	.0492280	.0678992	.0811709	.0908511	.1604021
.100	.0164799	.0108380	.0099579	.0181993	.0324791	.0470714	.0598326	.0792683	.0927843	.1027854	.1725022
.200	.0295578	.0200108	.0215633	.0384407	.0572754	.0730870	.0859917	.1061929	.1218411	.1345500	.1886242
.400	.0589683	.0430487	.0419852	.0727369	.0868785	.0809944	.0941780	.1163542	.1322169	.1428858	.1649840
.600	.0886999	.0618003	.0628494	.0942726	.0852757	.0785814	.0909043	.1092955	.1202343	.1266185	.1377852
.800	.1166680	.0771590	.0801377	.0959273	.0824680	.0739032	.0838645	.0973754	.1047153	.1088260	.1165024
1.000	.1429589	.0906911	.0861651	.0935635	.0794659	.0684010	.0759168	.0857228	.0909510	.0938616	.1002729

TABLE V.- CIRCULATION FUNCTION H

[Real part of $\bar{Q} = H + iJ$]

k	Values of H										
	A = 1	A = $1\frac{1}{2}$	A = 2	A = 3	A = 4	A = 5	A = 6	A = 8	A = 10	A = 12	A = ∞
0.00001	0.3509143	0.4337521	0.4963785	0.5887739	0.6543629	0.7029450	0.7400798	0.7926511	0.8278241	0.8529007	0.9999843
.0001	.3509019	.4337511	.4963490	.5887290	.6543056	.7028779	.7400044	.7925634	.8277282	.8527993	.9998421
.0010	.3507779	.4335211	.4960554	.5882857	.6537419	.7022178	.7392683	.7917160	.8268093	.8518305	.9983826
.0015	.3507103	.4334057	.4958945	.5880447	.6534358	.7018622	.7388735	.7912700	.8263313	.8513329	.9975516
.0020	.3506427	.4332919	.4957357	.5878069	.6531361	.7015146	.7384909	.7908403	.8258756	.8508660	.9967096
.0025	.3505756	.4331786	.4955778	.5875726	.6528424	.7011769	.7381192	.7904278	.8254429	.8504267	.9958582
.003	.3505093	.4330666	.4954226	.5873421	.6525542	.7008462	.7377592	.7900324	.8250346	.8500184	.9949986
.004	.3503779	.4328457	.4951166	.5868917	.6519957	.7002114	.7370723	.7892937	.8242863	.8492842	.9932579
.005	.3502483	.4326285	.4948177	.5864565	.6514611	.6996112	.7364321	.7886204	.8236236	.8486579	.9914931
.006	.3501207	.4324157	.4945257	.5860347	.6509512	.6990444	.7358353	.7880135	.8230475	.8481319	.9897082
.008	.3498708	.4320017	.4939622	.5852361	.6500002	.6980125	.7347704	.7869814	.8221212	.8473443	.9860897
.010	.3496284	.4316029	.4934252	.5844935	.6491421	.6971066	.7338681	.7861753	.8214640	.8468432	.9824215
.012	.3493927	.4312195	.4929149	.5838059	.6483710	.6963221	.7331173	.7855651	.8210221	.8465458	.9787174
.016	.3489411	.4304968	.4919719	.5825911	.6470783	.6950844	.7320145	.7848102	.8205686	.8462662	.9712418
.020	.3485149	.4298512	.4911273	.5815759	.6460869	.6942297	.7313454	.7844710	.8203770	.8460056	.9637252
.024	.3481128	.4292199	.4903770	.5807438	.6453585	.6936852	.7309890	.7843273	.8201495	.8454521	.9562111
.028	.3477339	.4286609	.4897152	.5800796	.6448550	.6933771	.7308316	.7841967	.8196931	.8444628	.9487308
.032	.3473769	.4281510	.4891375	.5795652	.6445297	.6932332	.7307753	.7839521	.8189122	.8430159	.9413079
.036	.3470412	.4276885	.4886382	.5791830	.6443494	.6931897	.7307342	.7835113	.8177748	.8411443	.9339603
.040	.3467254	.4272716	.4882125	.5789148	.6442771	.6931928	.7306450	.7828512	.8162954	.8389135	.9267018
.050	.3460205	.4264124	.4874370	.5786356	.6443481	.6931161	.7299361	.7800409	.8113385	.8322168	.9090090
.060	.3454256	.4257898	.4870107	.5787216	.6444573	.6925775	.7283065	.7759042	.8051518	.8246145	.8920397
.080	.3445296	.4251296	.4869125	.5792151	.6438170	.6895166	.7224559	.7651893	.7912387	.8087496	.8604318
.100	.3439684	.4250595	.4873943	.5793174	.6415172	.6841635	.7143703	.7532551	.7771568	.7934125	.8319241
.200	.3443291	.4277824	.4888370	.5688207	.6169002	.6486244	.6713884	.7008314	.7186352	.7297453	.7275799
.400	.3492206	.4281282	.4783674	.5589592	.5754428	.5999455	.6163212	.6331816	.6395591	.6410756	.6249763
.600	.3527385	.4245519	.4681431	.5210524	.5523383	.5710141	.5826310	.5902297	.5912919	.5909145	.5788016
.800	.3552225	.4218555	.4619695	.5105718	.5374110	.5515280	.5598430	.5633572	.5632928	.5629860	.5541466
1.000	.3574376	.4205666	.4585838	.5037746	.5267253	.5377109	.5444159	.5463965	.5462361	.5462562	.5394348

TABLE VI.- CIRCULATION FUNCTION -J

[Negative imaginary part of $\bar{Q} = H + iJ$]

k	Values of -J										
	A = 1	A = $1\frac{1}{2}$	A = 2	A = 3	A = 4	A = 5	A = 6	A = 8	A = 10	A = 12	A = ∞
0.00001	0.0000076	0.0000129	0.0000181	0.0000274	0.0000349	0.0000410	0.0000458	0.0000530	0.0000581	0.0000617	0.0001151
.0001	.0000565	.0000966	.0001353	.0002042	.0002604	.0003053	.0003409	.0003947	.0004321	.0004592	.0009323
.0010	.0003624	.0006209	.0008698	.0013111	.0016688	.0019538	.0021771	.0025182	.0027545	.0029249	.0070017
.0015	.0004900	.0008403	.0011771	.0017732	.0022556	.0026397	.0029397	.0033997	.0037185	.0039485	.0098776
.0020	.0006026	.0010342	.0014486	.0021811	.0027732	.0032443	.0036115	.0041766	.0045689	.0048528	.0125797
.0025	.0007041	.0012093	.0016937	.0025489	.0032395	.0037889	.0042162	.0048768	.0053367	.0056710	.0151455
.003	.0007969	.0013693	.0019176	.0028847	.0036651	.0042859	.0047682	.0055170	.0060406	.0064236	.0176028
.004	.0009614	.0016557	.0023156	.0034809	.0044204	.0051682	.0057486	.0066592	.0073038	.0077657	.0222566
.005	.0011039	.0019007	.0026610	.0039979	.0050757	.0059350	.0066023	.0076628	.0084262	.0090081	.0266298
.006	.0012290	.0021179	.0029649	.0044527	.0056528	.0066124	.0073594	.0085642	.0094504	.0101445	.0307752
.008	.0014380	.0024825	.0034750	.0052174	.0066279	.0077661	.0086611	.0101569	.0113154	.0122777	.0385130
.010	.0016041	.0027741	.0038838	.0058338	.0074237	.0087245	.0097646	.0115764	.0130606	.0143607	.0456521
.012	.0017364	.0030086	.0042138	.0063378	.0080884	.0095473	.0107403	.0129103	.0147845	.0164941	.0523015
.016	.0019224	.0033457	.0046944	.0070998	.0091487	.0109414	.0124902	.0155409	.0183901	.0210941	.0644043
.020	.0020276	.0035490	.0049966	.0076338	.0099887	.0121722	.0141695	.0185314	.0223634	.0261853	.0752079
.024	.0020707	.0036517	.0051693	.0080215	.0107208	.0133755	.0159238	.0213940	.0267156	.0316438	.0849491
.028	.0020642	.0036761	.0052459	.0083193	.0114207	.0146358	.0178302	.0247412	.0313549	.0372806	.0937910
.032	.0020171	.0036385	.0052509	.0085681	.0121403	.0160026	.0199202	.0283303	.0361571	.0429235	.1018541
.036	.0019562	.0035514	.0052031	.0087990	.0129145	.0175011	.0221948	.0320934	.0410033	.0484432	.1092323
.040	.0018266	.0034247	.0051174	.0090348	.0137654	.0191388	.0246353	.0359564	.0457962	.0537556	.1160013
.050	.0014536	.0029832	.0048110	.0097492	.0162914	.0237875	.0312559	.0456284	.0571354	.0658775	.1306444
.060	.0009753	.0024324	.0044736	.0107514	.0193759	.0290035	.0381900	.0547641	.0671969	.0762763	.1425944
.080	.0001757	.0012308	.0040097	.0137416	.0266753	.0398769	.0513824	.0702765	.0834026	.0927226	.1604021
.100	.0014589	.0001192	.0040554	.0177541	.0343847	.0498818	.0624478	.0821058	.0954355	.1050054	.1723022
.200	.0075503	.0016775	.0102371	.0377571	.0604216	.0775479	.0899776	.1106139	.1260349	.1380640	.1886242
.400	.0141291	.0020452	.0202440	.0489963	.0697264	.0863779	.0990876	.1223563	.1380032	.1476872	.1649840
.600	.0174692	.0024624	.0202039	.0465807	.0669941	.0839840	.0959111	.1158580	.1266589	.1319624	.1377852
.800	.0204211	.0003529	.0170811	.0425289	.0629263	.0789253	.0885879	.1041121	.1114867	.1145121	.1165024
1.000	.0233443	.0025349	.0135635	.0388535	.0586282	.0728613	.0802190	.0925226	.0979647	.0998266	.1002729

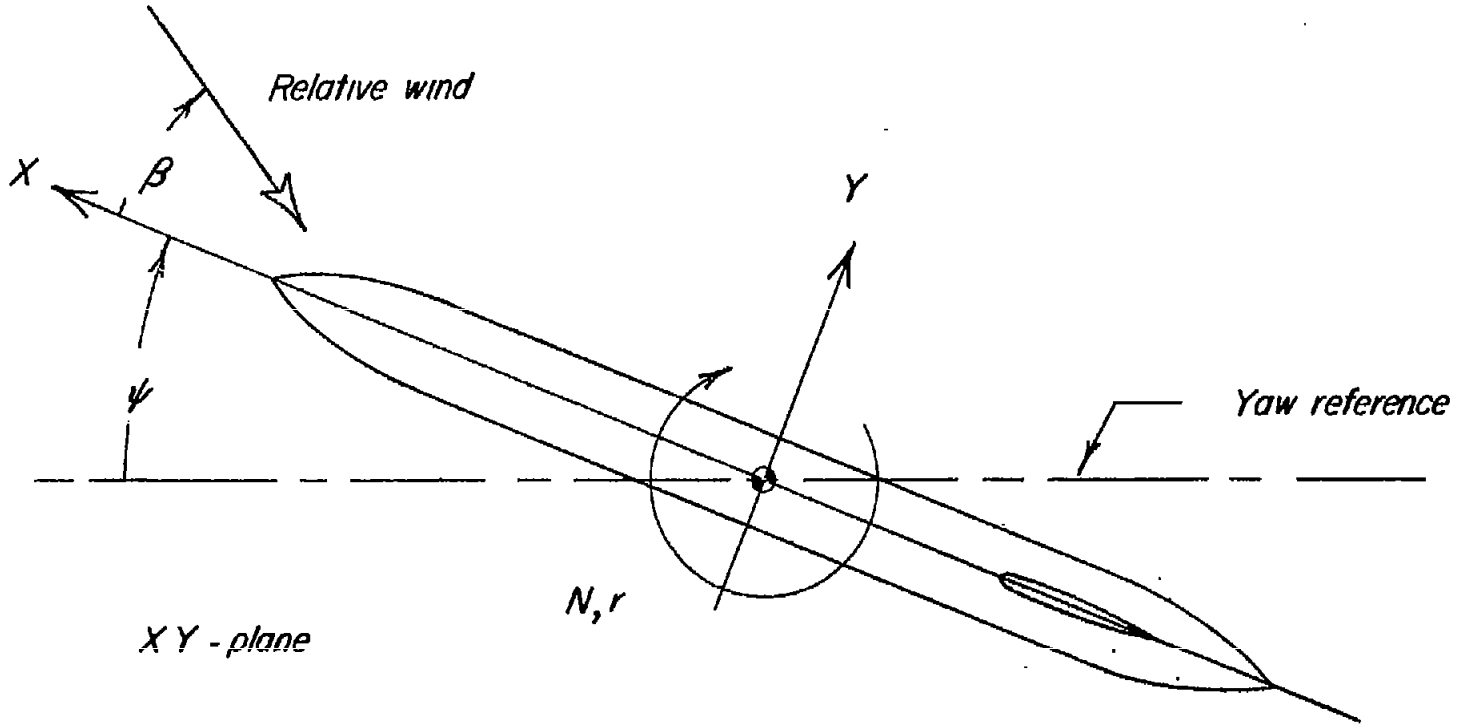

Figure 1.- System of stability axes. Arrows indicate positive forces, moments, and angular displacements. Yaw reference is generally chosen to coincide with initial relative wind.

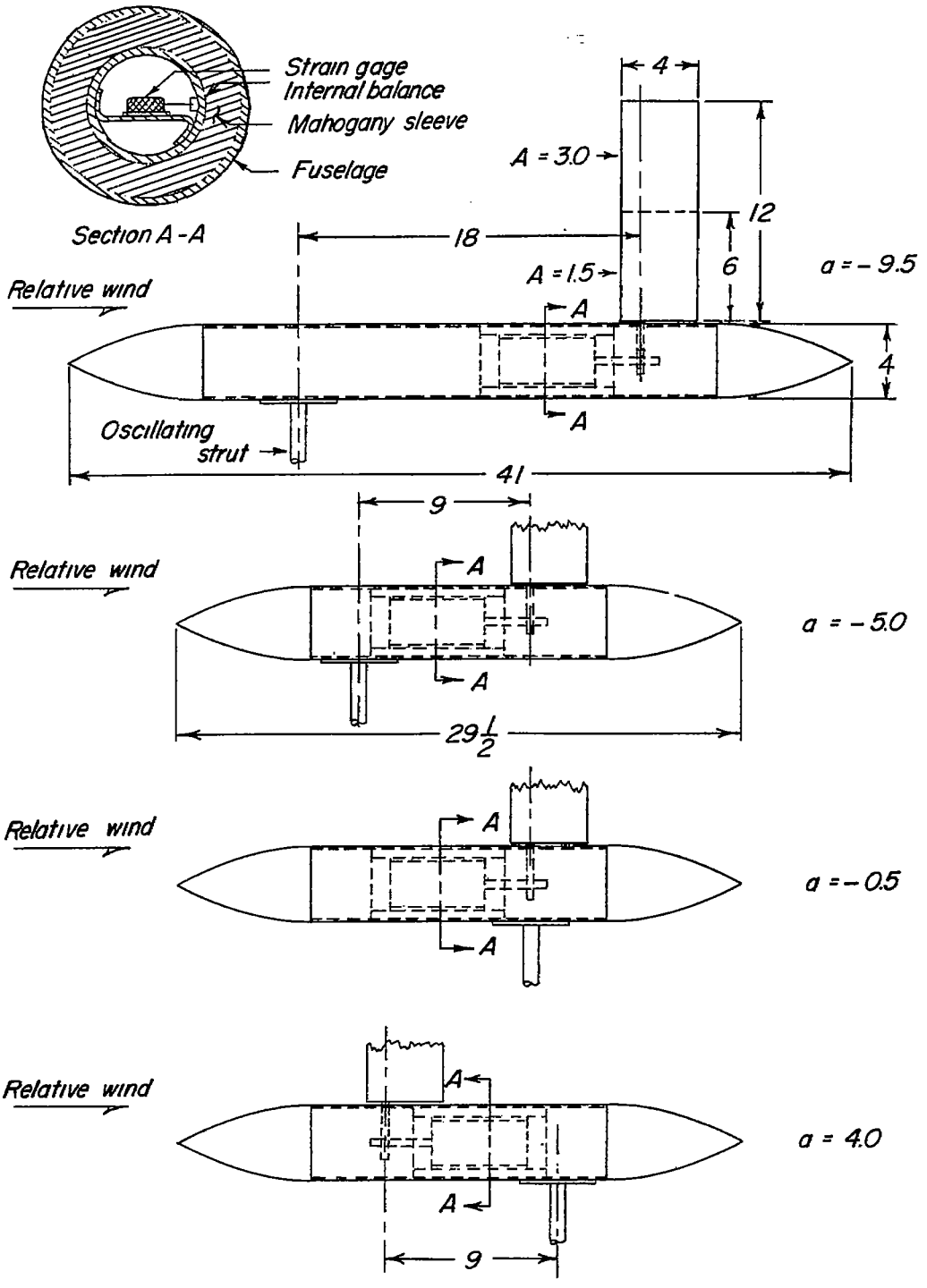

Figure 2.- Configurations of the model tested. All dimensions are in inches.

$\frac{c_t}{b_w} = 0.12$; $\frac{S_t}{S_w} = 0.26$ for A = 3.0; $\frac{S_t}{S_w} = 0.13$ for A = 1.5.

L-66494

Figure 3.- Test model on forced-oscillation strut in Langley stability tunnel. A = 3.0; a = -9.5.

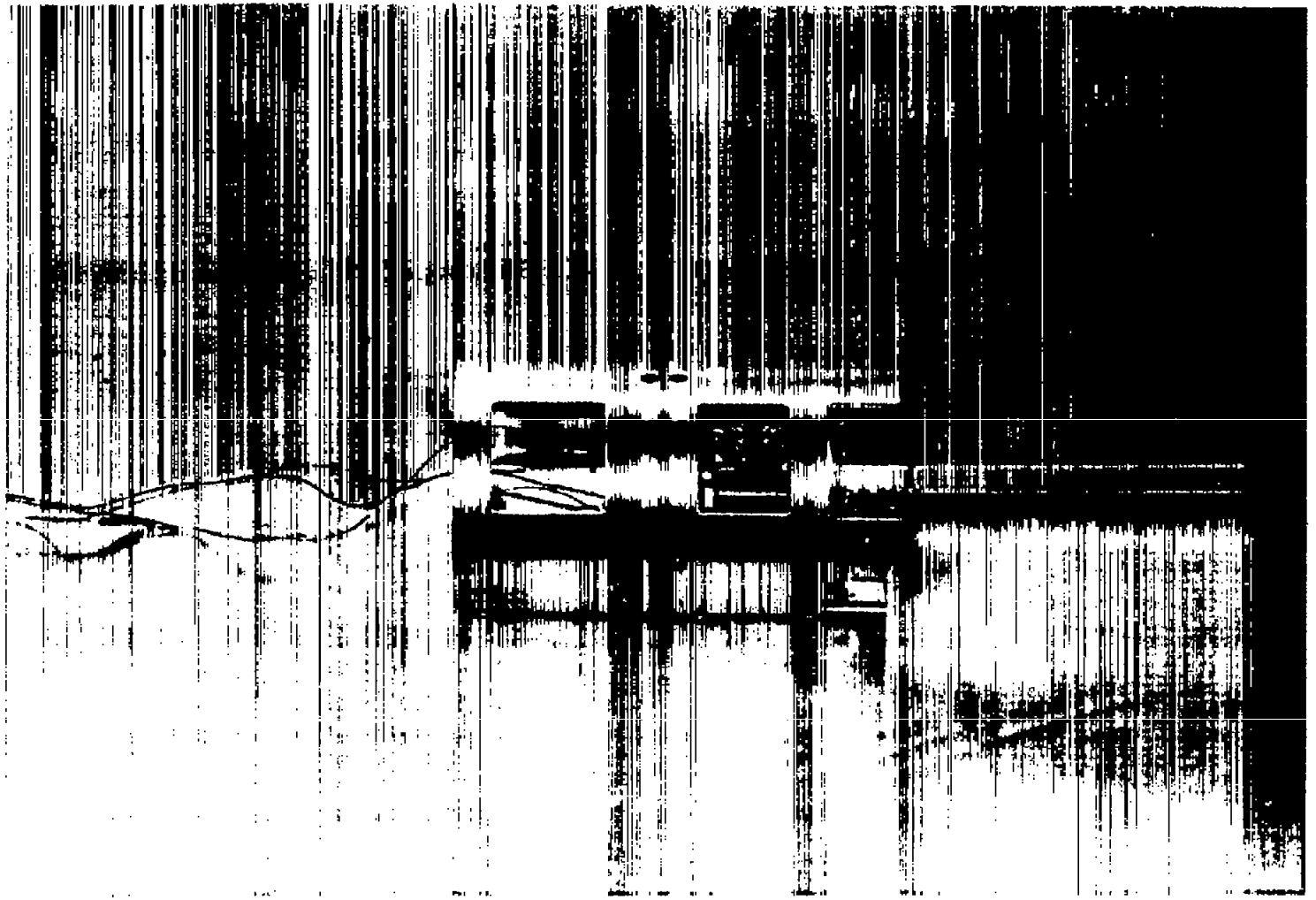

L-64656

Figure 4.- The fuselage-contained strain-gage balance used to measure forces on vertical tail.

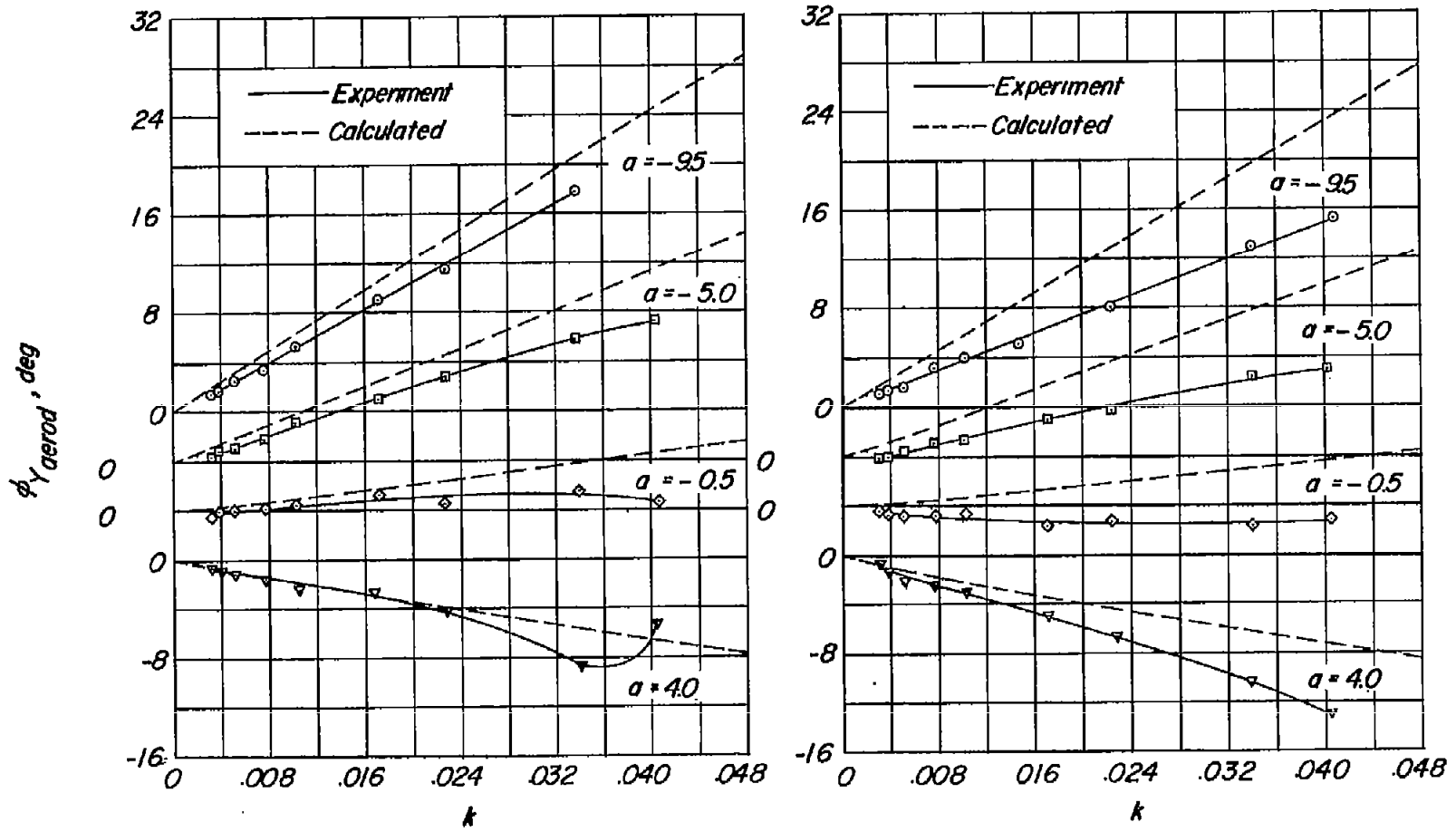

(a) A = 1.5. (b) A = 3.0.

Figure 5.- Experimental and calculated effects of reduced-frequency parameter on phase angle between tail force and displacement for four tail lengths and two vertical-tail aspect ratios.

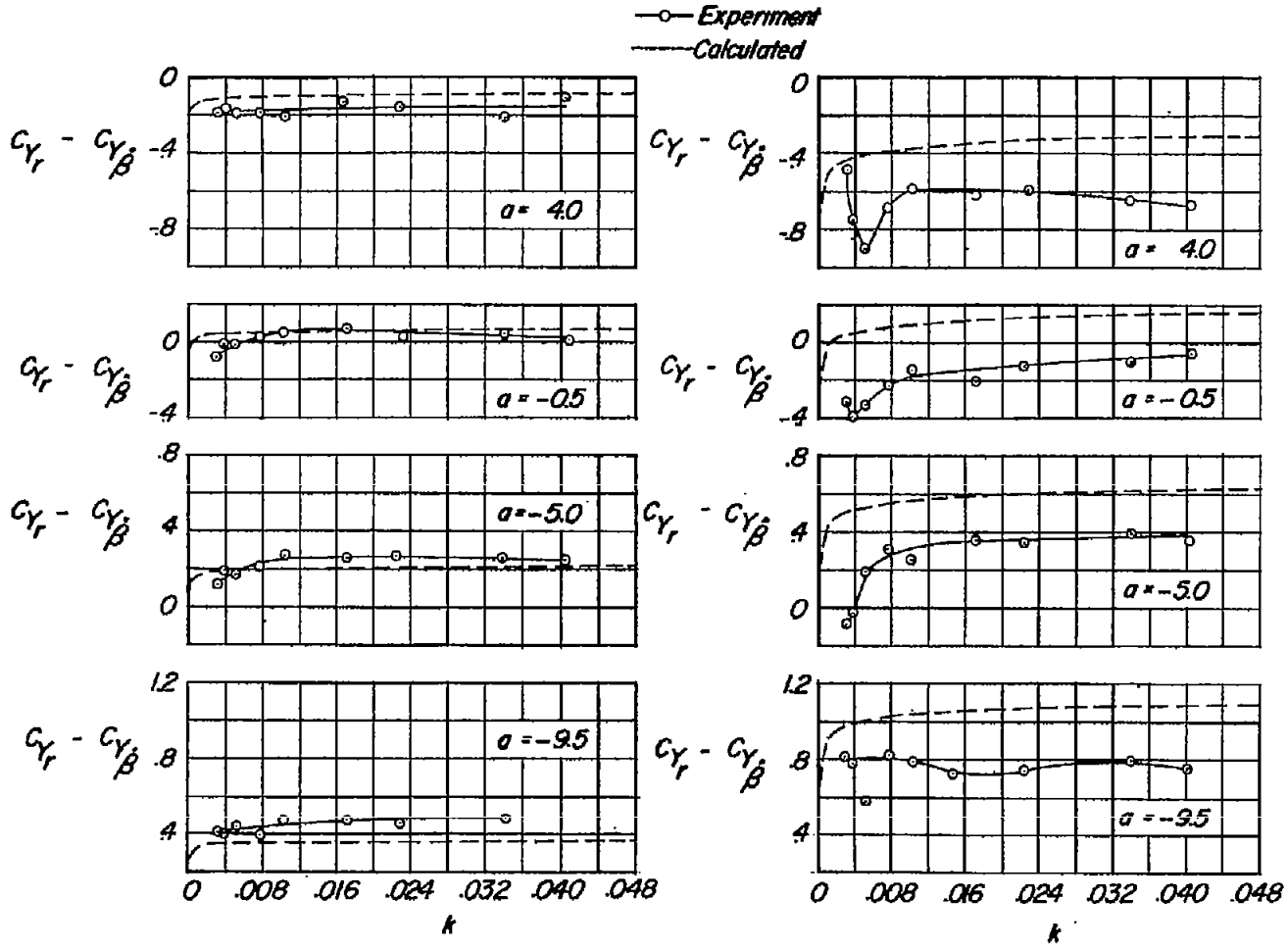

(a) A = 1.5. (b) A = 3.0.

Figure 6.- Experimental and calculated effects of reduced-frequency parameter on lateral force due to yawing for four tail lengths and two vertical-tail aspect ratios.

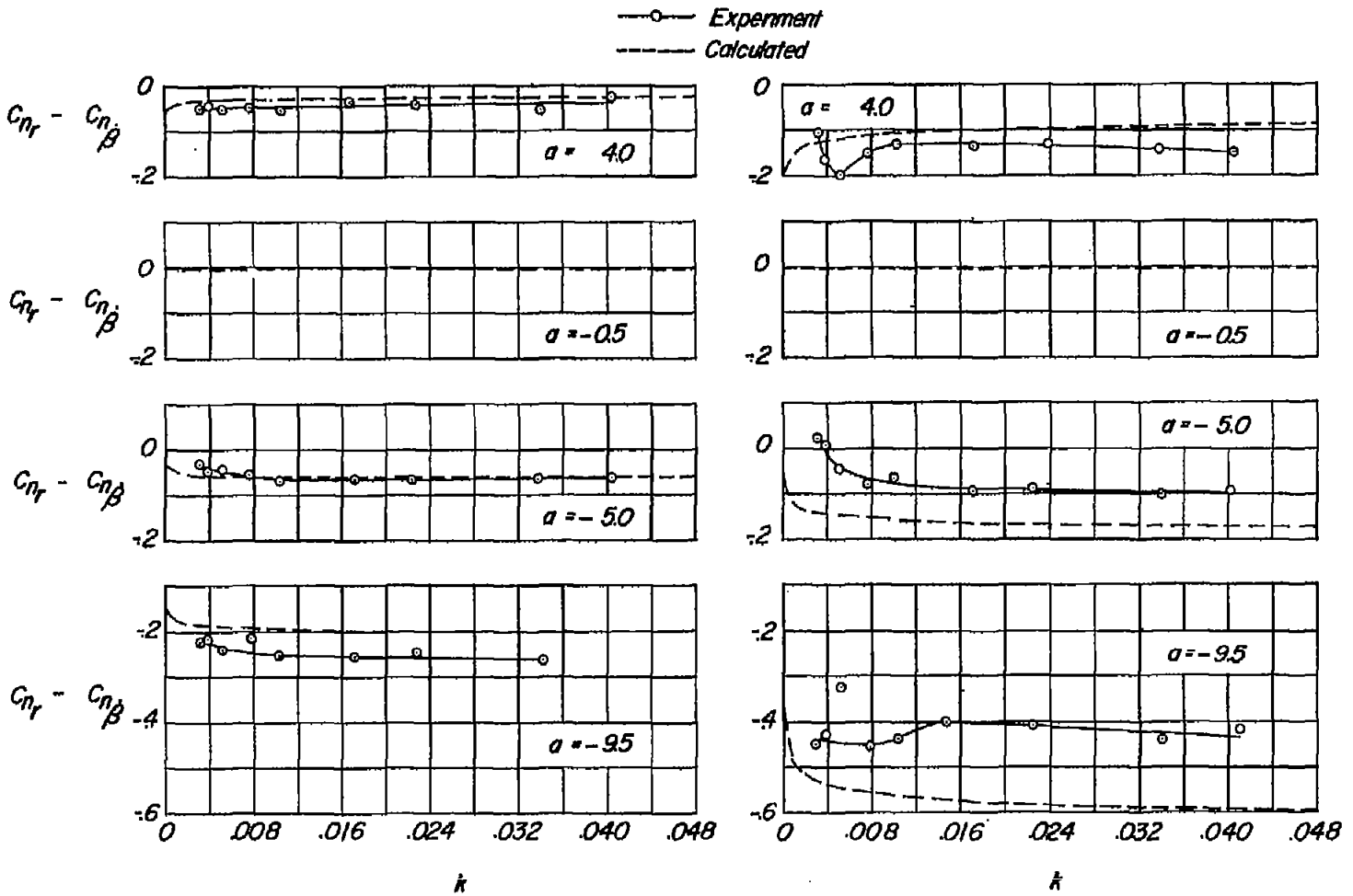

(a) A = 1.5. (b) A = 3.0.

Figure 7.- Experimental and calculated effects of reduced-frequency parameter on the damping in yaw for four tail lengths and two vertical-tail aspect ratios.

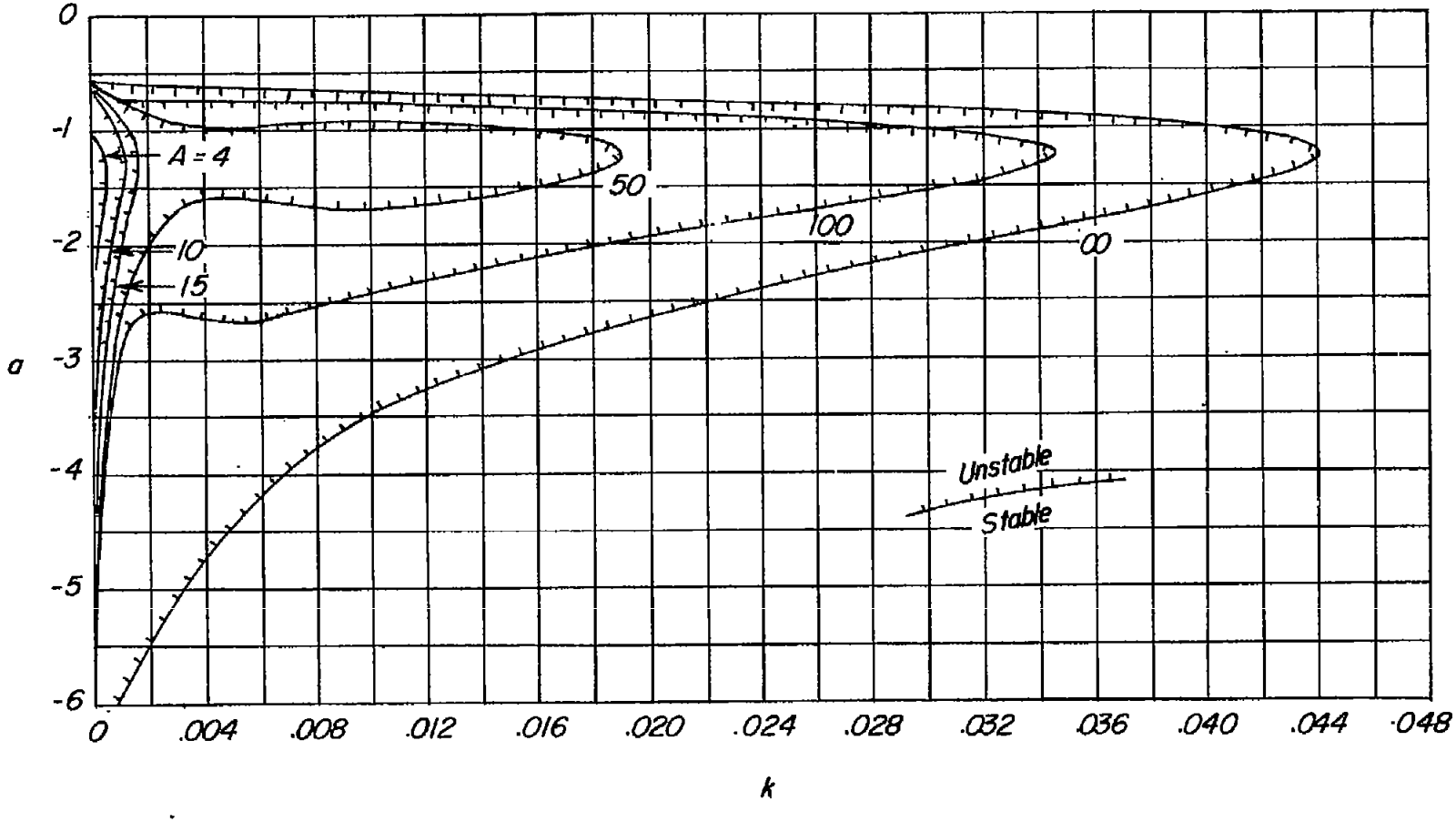

Figure 8.- Boundaries of lateral damping due to vertical tail. Curves represent conditions of tail-length and reduced-frequency parameters for which the damping in yaw is zero.

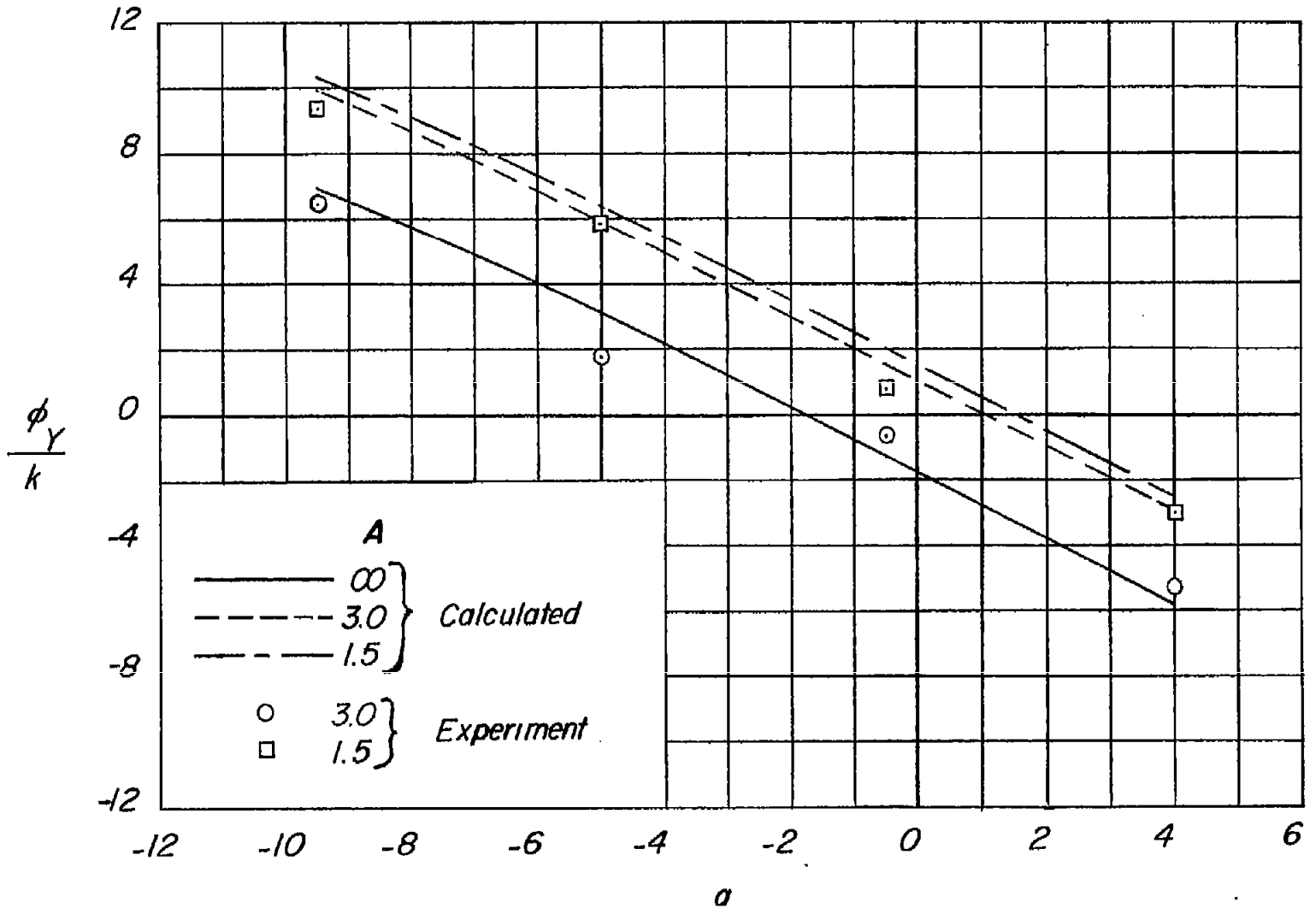

Figure 9.- Variation of ϕ_Y/k with tail-length parameter. k = 0.05.

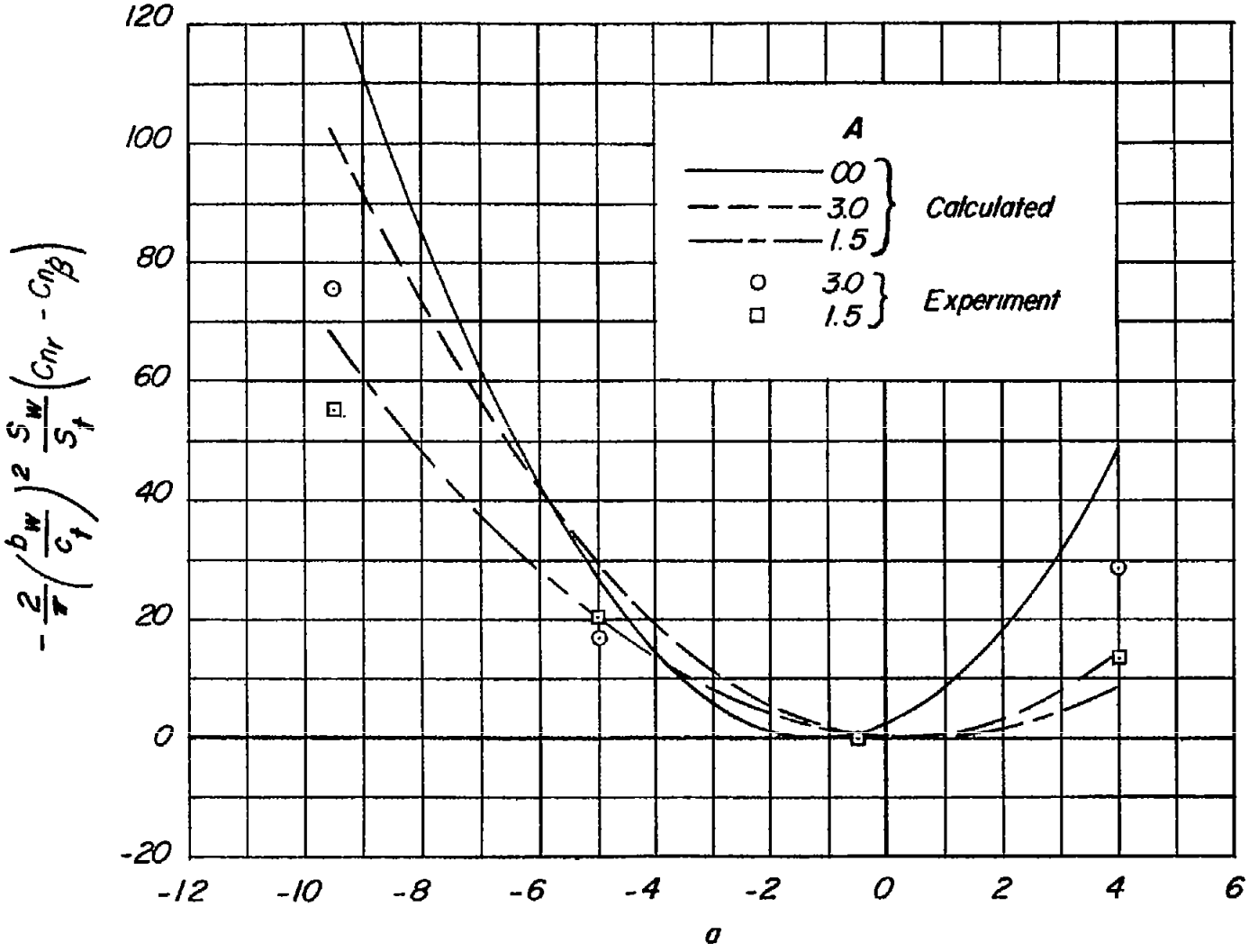

Figure 10.- Variation of damping-in-yaw parameter with tail-length parameter. k = 0.05.

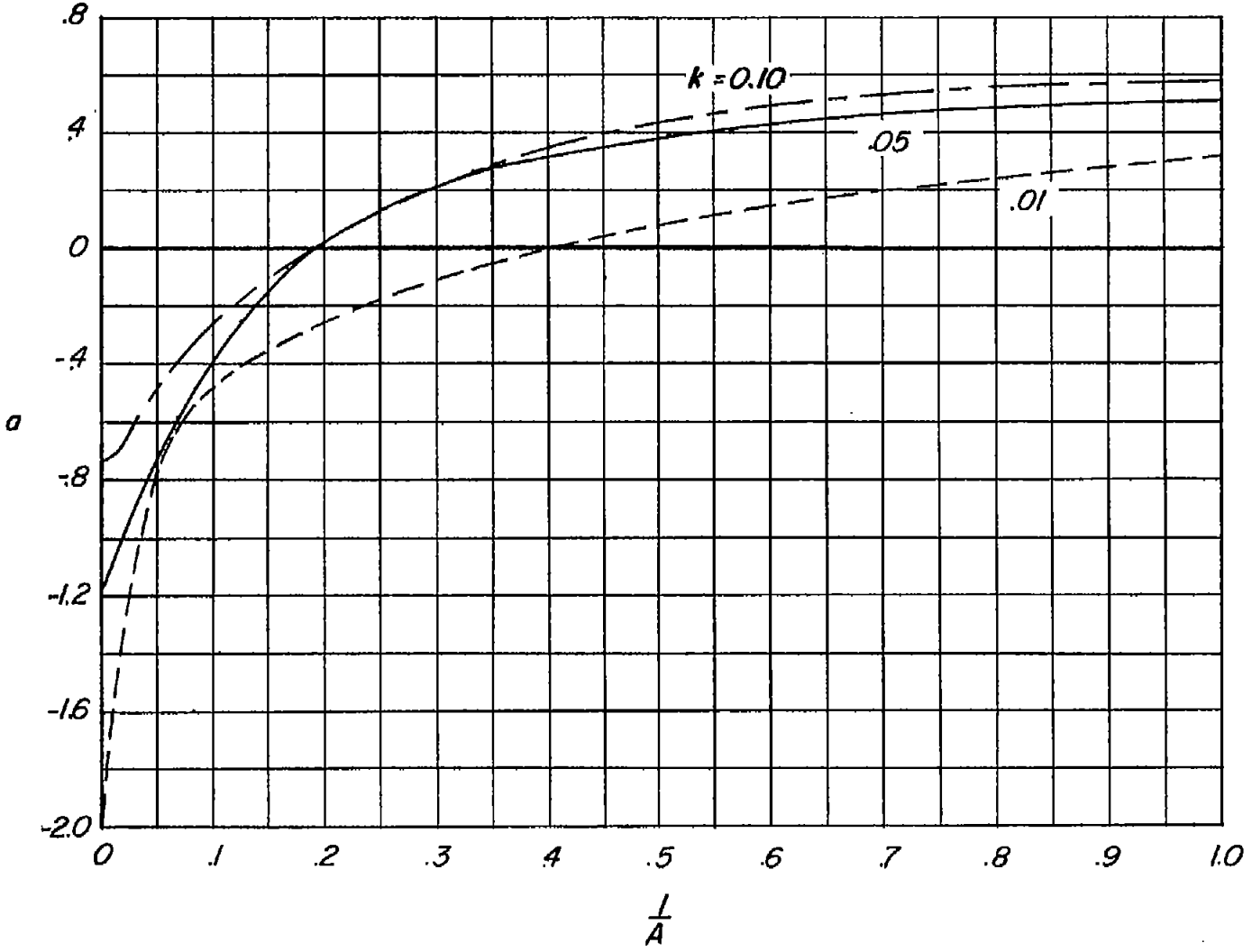

Figure 11.- Values of tail-length parameter for which damping in yaw is minimum.

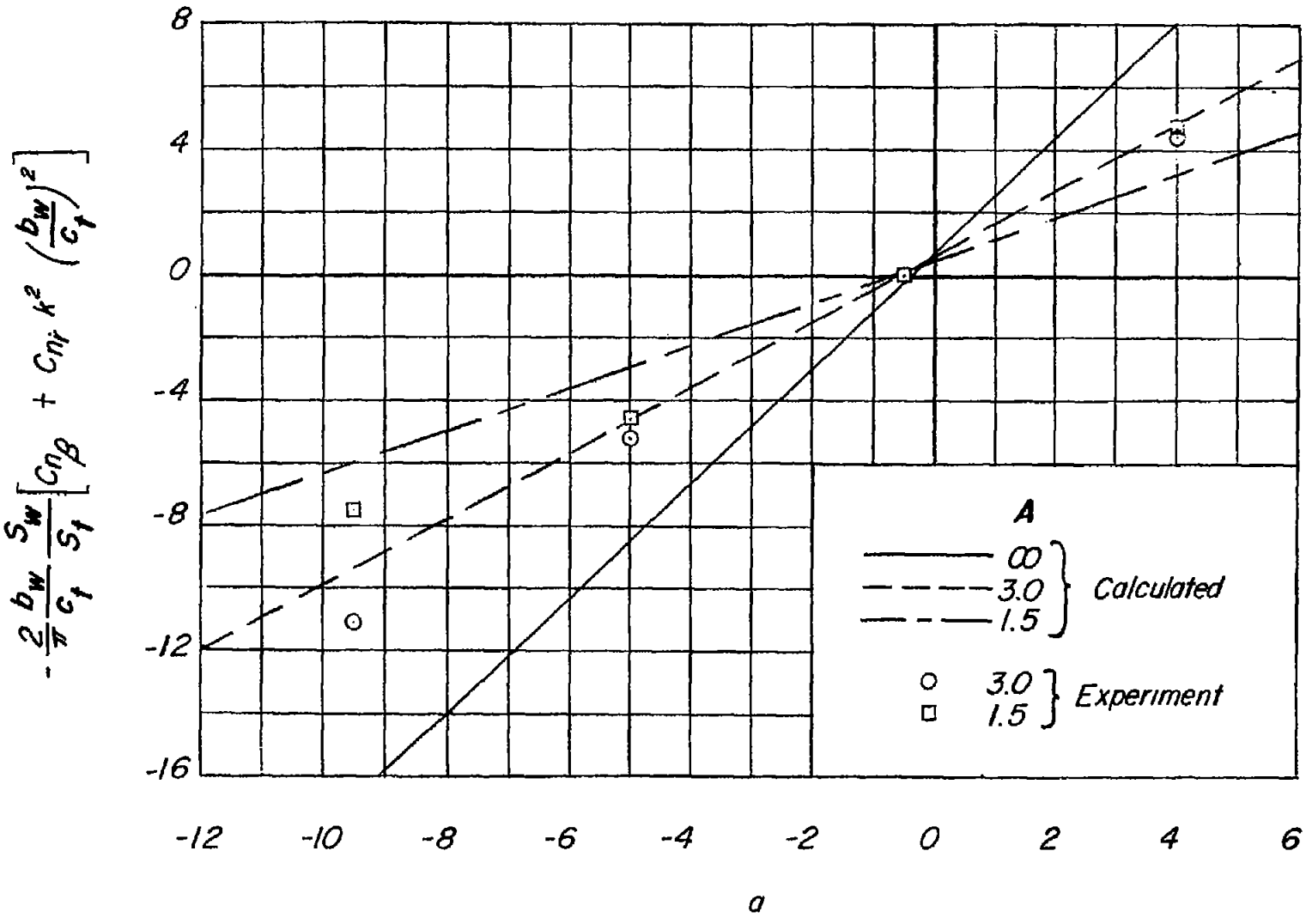

Figure 12.- Variation of directional-stability parameter with normal values of tail-length parameter. k = 0.05.

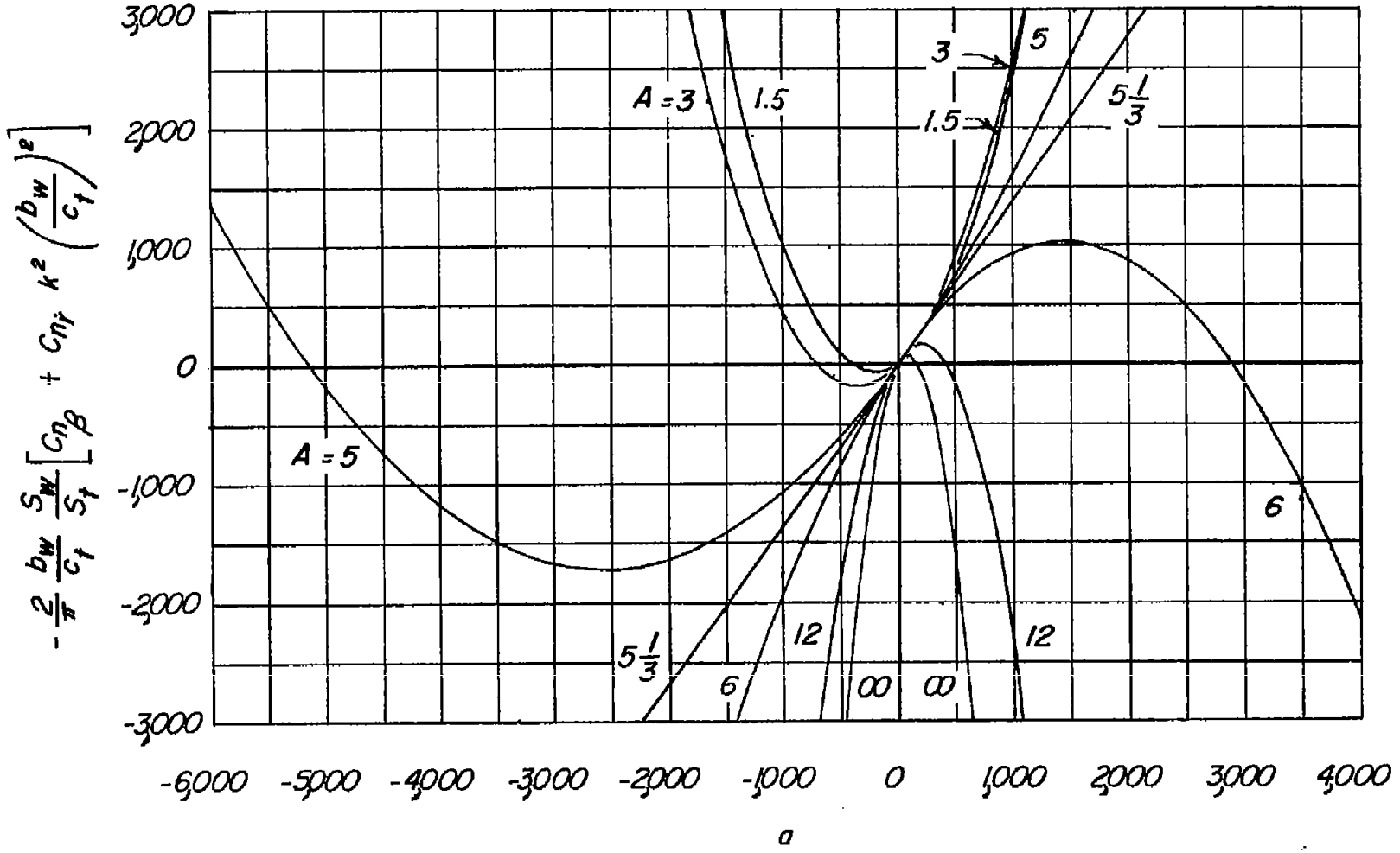

Figure 13.- Variation of directional-stability parameter with extremely large values of tail-length parameter. Numbers represent vertical-tail aspect ratio. k = 0.05.

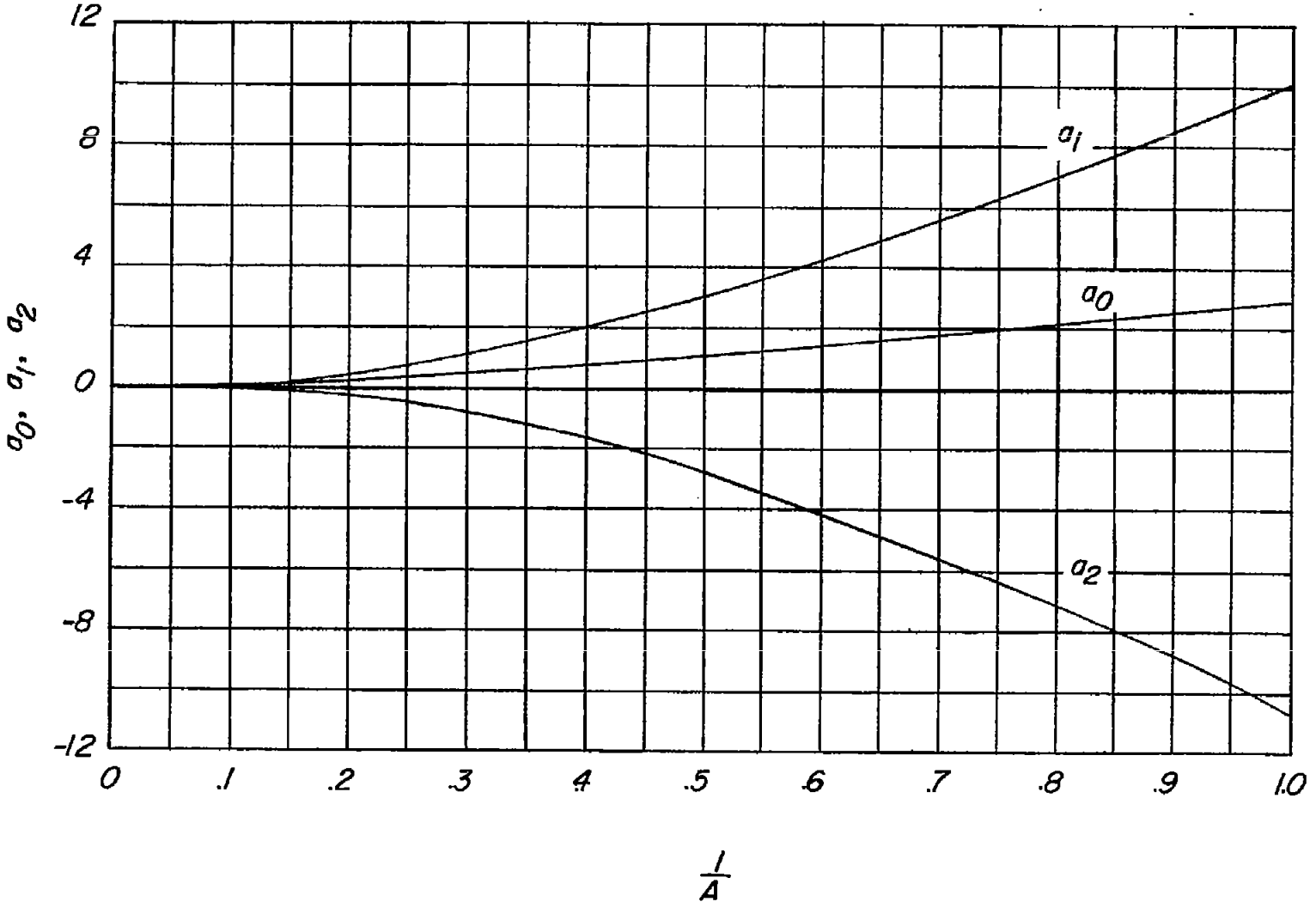

Figure 14.- Variation with aspect ratio of aspect-ratio functions a_0, a_1, and a_2 used in computation of $\bar{P}$ and $\bar{Q}$.

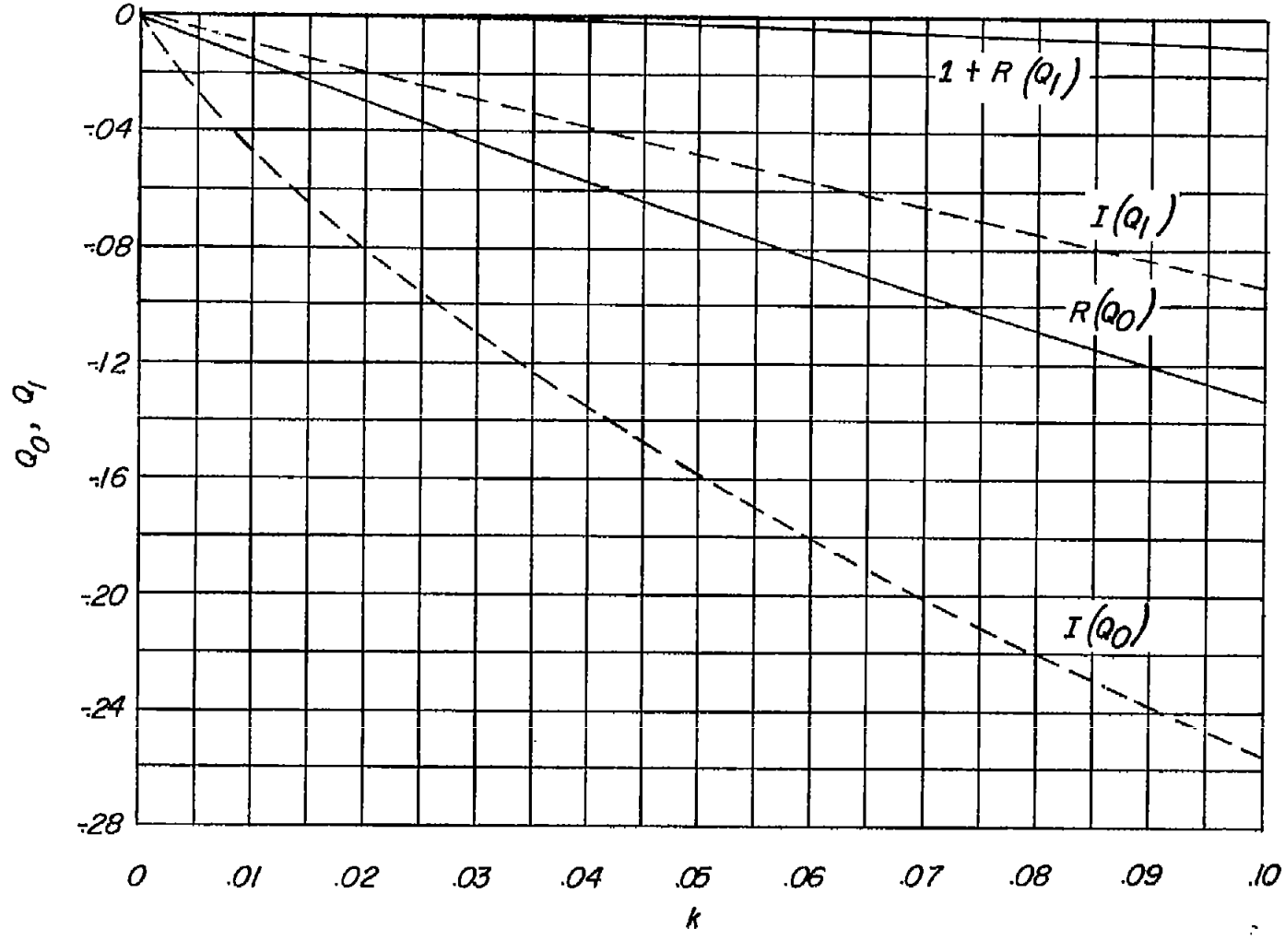

Figure 15.- Variation with reduced-frequency parameter of complex frequency functions Q_0 and Q_1 used in the computations of $\overline{P}$ and $\overline{Q}$.

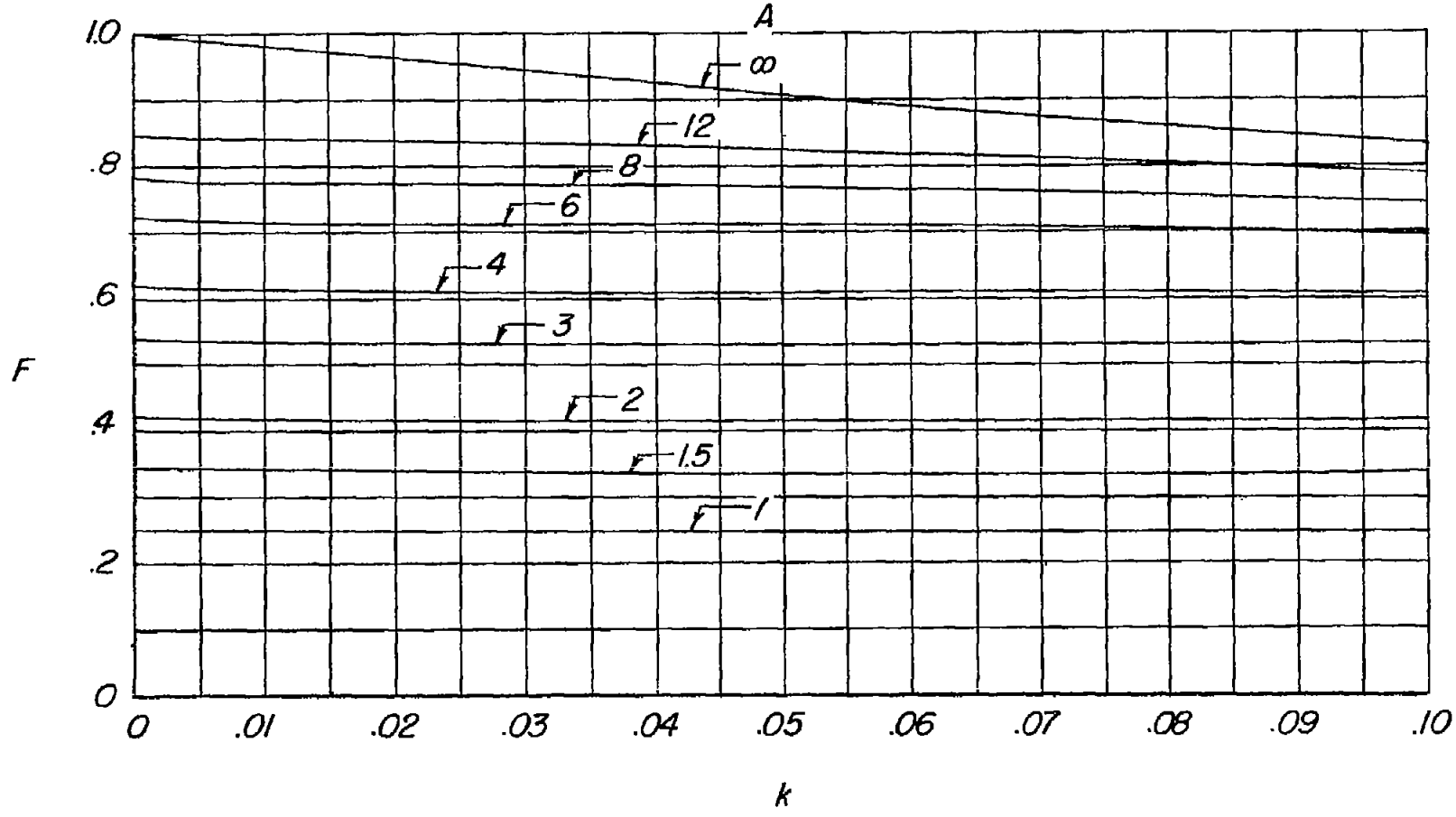

Figure 16.- Effect of reduced-frequency parameter on unsteady-circulation function F, the real part of $\bar{F}$.

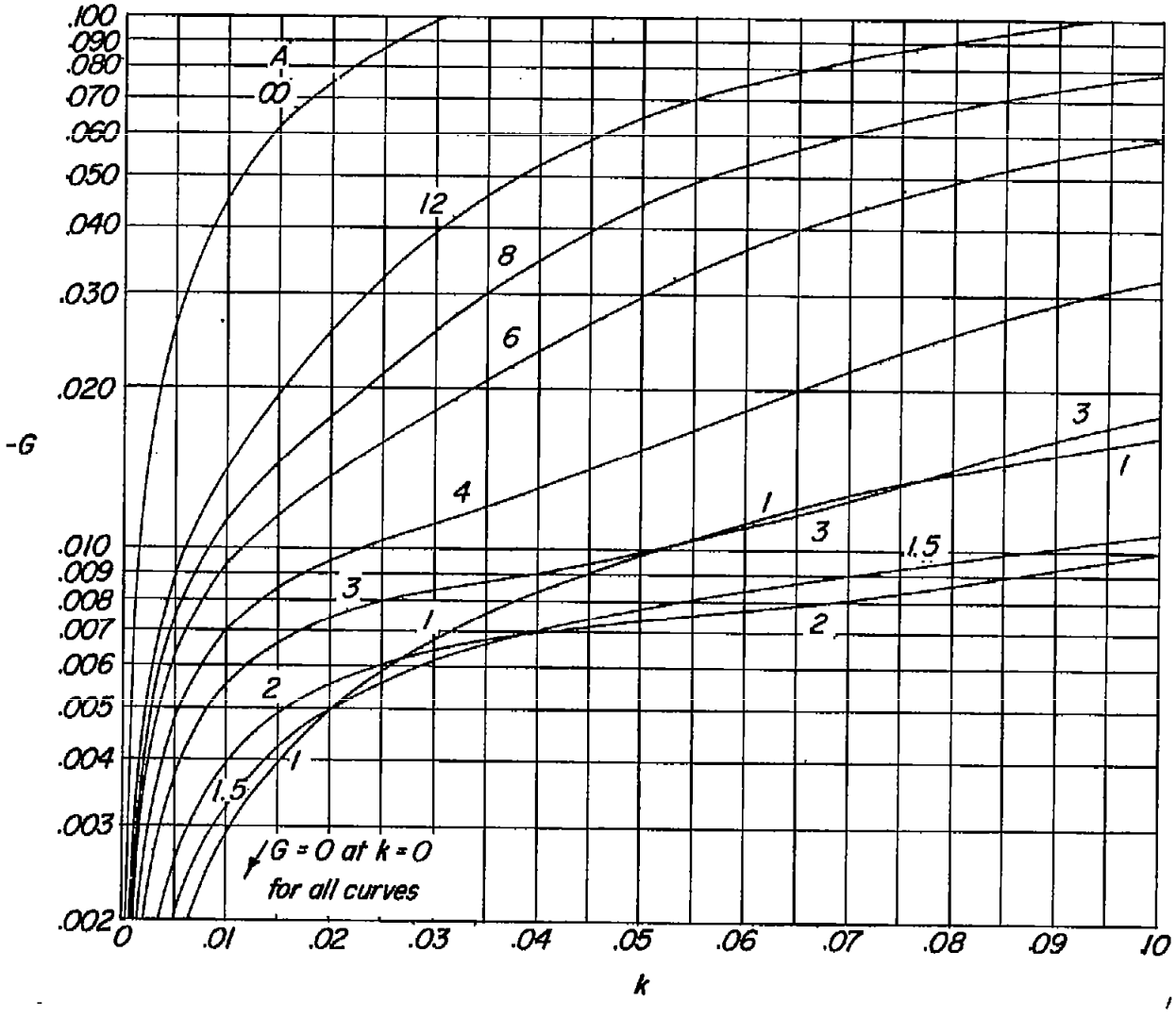

Figure 17.- Effect of reduced-frequency parameter on unsteady-circulation function G, the imaginary part of $\overline{P}$.

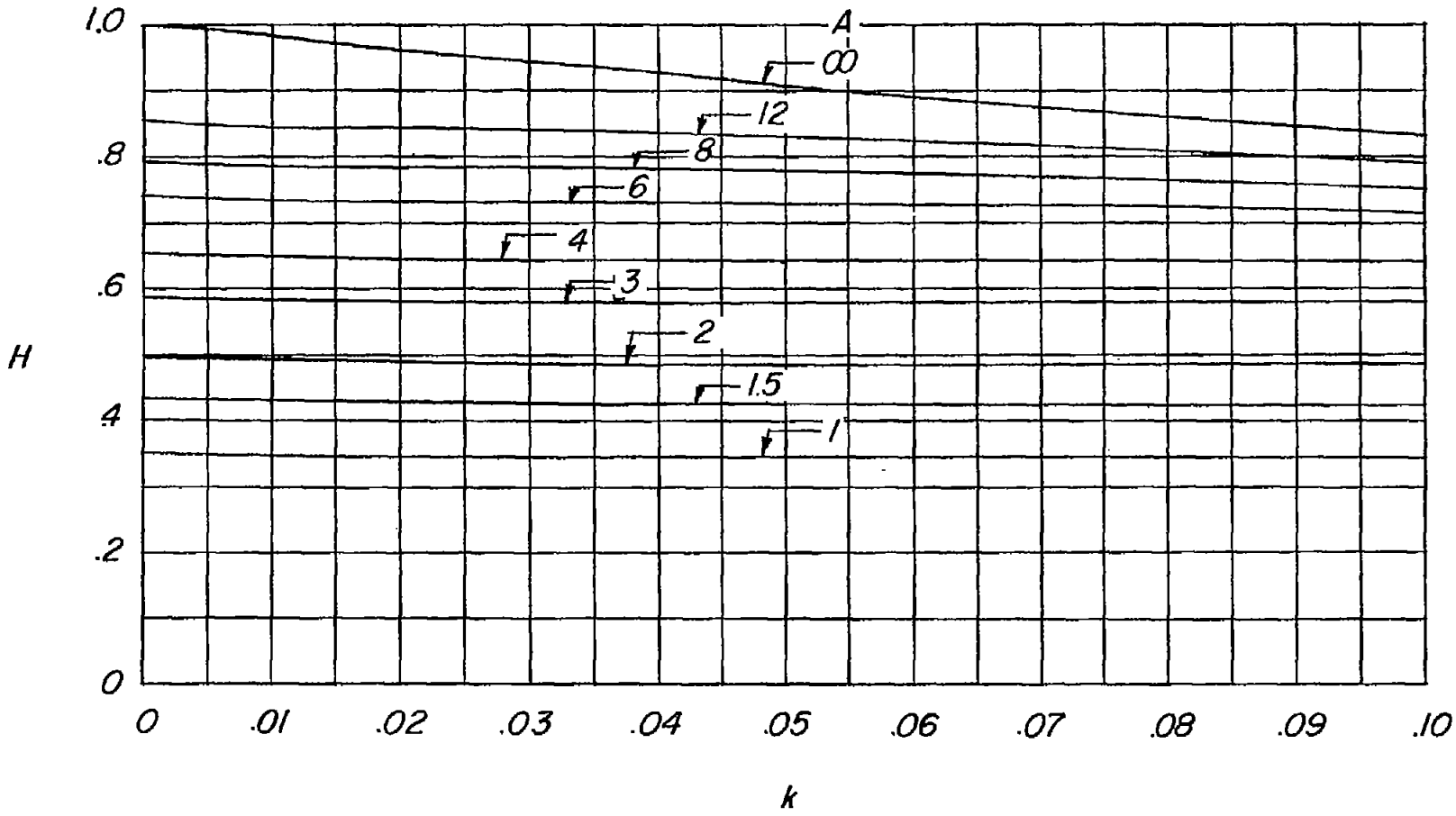

Figure 18.- Effect of reduced-frequency parameter on unsteady-circulation function H, the real part of $\overline{Q}$.

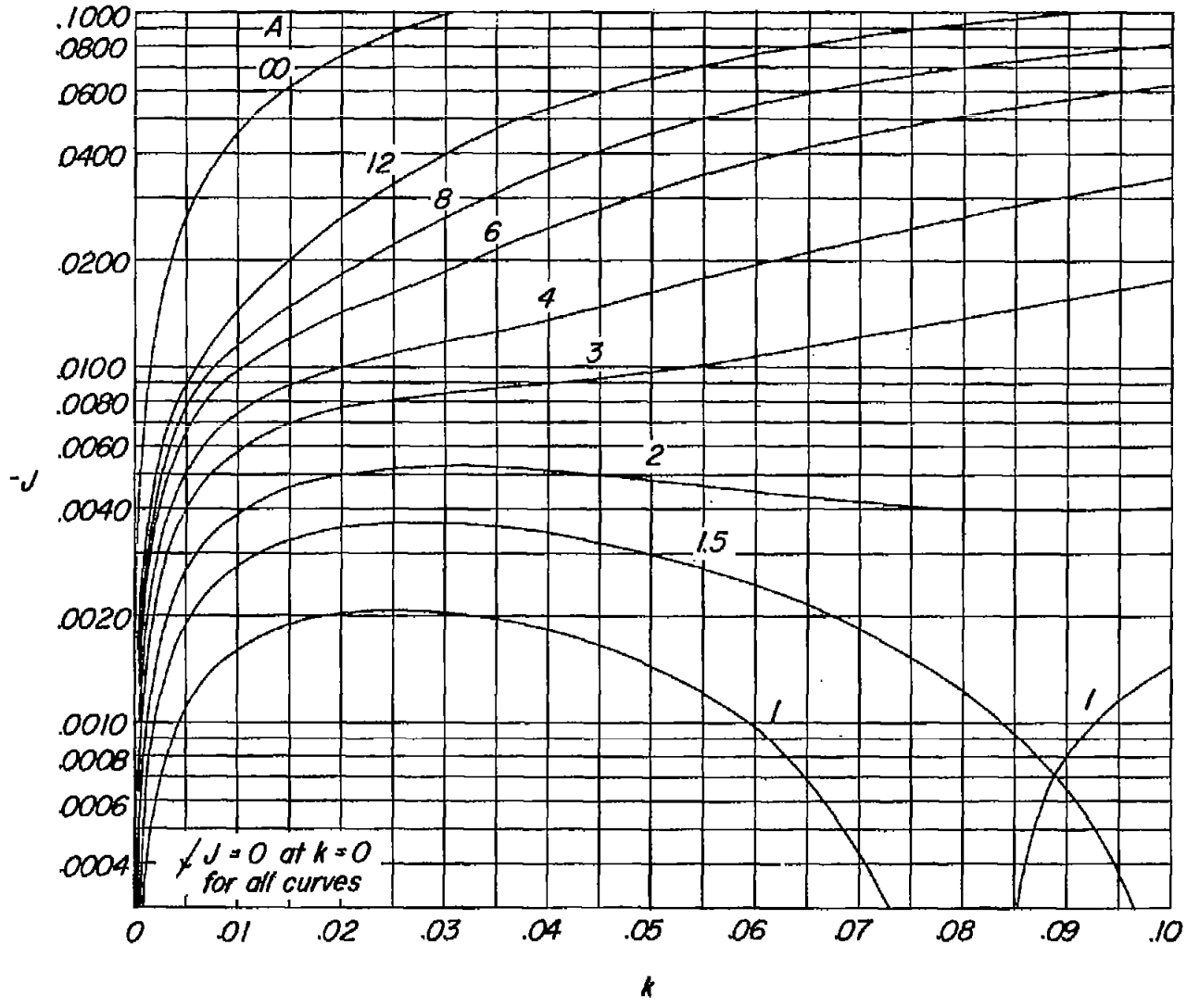

Figure 19.- Effect of reduced-frequency parameter on unsteady-circulation function J, the imaginary part of $\overline{Q}$.